# Chapter 8
# Hierarchical Nanomechanics of Collagen Fibrils: Atomistic and Molecular Modeling

**M.J. Buehler**

**Abstract** This chapter describes hierarchical multi-scale modeling of collagenous tissues, with a particular focus on the mechanical properties. Studies focus on elastic behavior, plastic behavior and fracture. Starting at the atomistic scale, we review development and application of a hierarchical multi-scale model that is capable of describing the dynamical behavior of a large number of tropocollagen molecules, reaching length scales of several micrometers and time scales of tens of microseconds. Particular emphasis is on elucidating the deformation mechanisms that operate at various scales, the scale-dependent properties, the effect of specific hierarchical features and length scales (cross-link densities, intermolecular adhesion, etc.) as well as on the effect of addition of mineral platelets during formation of nascent bone. This chapter contains a review of numerical techniques associated with modeling of chemically complex and hierarchical biological tissue, including first principles-based reactive force fields, empirical force fields, large-scale parallelization and visualization methods. A set of scaling relationships are summarized that enable one to predict deformation mechanisms and properties based on atomistic, molecular and other hierarchical features. The results are presented in deformation maps that summarize deformation modes, strength, dissipative properties and elastic behavior for various conditions, providing structure–property relationships for collagenous tissue. This chapter is concluded with a discussion of how insight of nanomechanical behavior at the smallest scales relates with the physiological role of collagen. The significance of universal structural patterns such as the staggered collagen fibril architecture versus specific structures in different collagen tissues is reviewed in light of the question of universality versus diversity of structural components.

## 8.1 Introduction

Proteins are the fundamental building blocks of a vast array of biological materials that are involved in critical functions of life, many of which are based on highly characteristic nanostructured arrangements of protein components that include tropocollagen (here sometimes also abbreviated as "TC") molecules, alpha-helices or beta-sheets. Bone, providing structure to our body, or spider silk, used for prey

P. Fratzl (ed.), *Collagen: Structure and Mechanics*,
© Springer Science+Business Media, LLC 2008

procurement, are examples of materials that have incredible elasticity, strength and robustness unmatched by many synthetic materials, mainly attributed to its structural formation with molecular precision.

Collagen, the most abundant protein on earth, is a fibrous structural protein with superior mechanical properties, and provides an intriguing example of a hierarchical biological nanomaterial (Borel and Monboisse 1993; Hellmich and Ulm 2002; Puxkandl et al. 2002; Bhattacharjee and Bansal 2005; Bozec et al. 2005; Bozec and Horton 2005; Fratzl and Weinkamer 2007). The hierarchical structure of collagen is summarized in Fig. 8.1. Collagen plays an important role in many biological tissues, including tendon, bone, teeth, cartilage or in the eye's cornea focusing on small-scale structural features. Severe mechanical tensile loading of collagen is significant under many physiological conditions, as in joints and in bone. Further, significant mechanical deformation of collagenous tissues may occur during injuries.

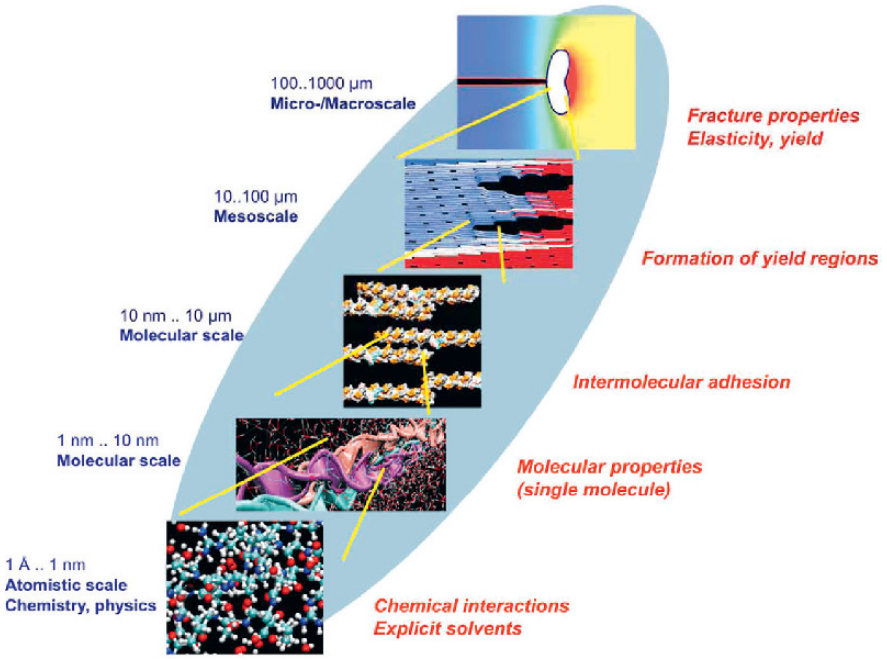


**Fig. 8.1** Overview of different material scales, from nano to macro, here exemplified for collagenous tissue (Ramachandran and Kartha 1955; Bhattacharjee and Bansal 2005; Hulmes et al. 1995; Puxkandl et al. 2002; An et al. 2004; Fratzl et al. 2004; Buehler 2006a,b). The macroscopic mechanical material behavior is controlled by the interplay of properties throughout various scales, in particular molecular interaction at the mesoscale. In order to understand deformation and fracture mechanisms, it is crucial to elucidate atomistic and molecular mechanisms at each scale

The goal of this chapter is to review the elastic, plastic and fracture behavior of collagen fibrils, linking atomistic-scale studies with the mesoscopic level of collagen fibrils. We particularly focus on the large deformation behavior of collagen-based tissues, which is particularly important under physiological conditions and

during injuries. The studies reviewed here explain the limiting factors in strength of collagen fibrils, as well as the origins of its toughness. These investigations complement experimental efforts focused on the deformation mechanics of collagen fibril at nanoscale, including characterization of changes of *D*-spacing and fibril orientation (Hulmes et al. 1995), analyses that featured X-ray diffraction and synchrotron radiation experiments (Puxkandl et al. 2002).

### *8.1.1 Deformation and Fracture: An Introduction*

When materials are deformed, they display a small regime in which deformation is reversible or elastic (Broberg 1990; Anderson 1991). Once the forces on the material reach a critical level, deformation becomes irreversible and remains even after the load is removed. This is referred to as the plastic regime (Courtney 1990). Plastic deformation is typically followed by fracture, when the material breaks and fails. Many materials, including metals, ceramics, polymers and biological tissue, show this generic behavior. However, the details of the response to mechanical load depend on the atomic and molecular makeup of the material; from nano to macro (for a review on this topic, please see Buehler and Ackbarow 2007) (see Fig. 8.2).

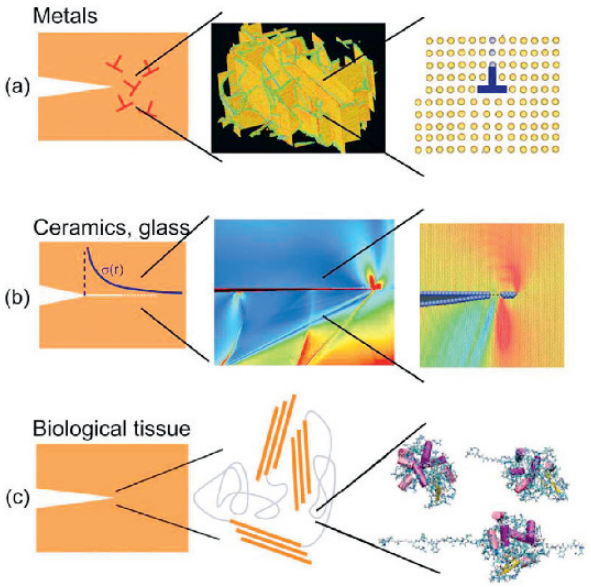


**Fig. 8.2** Overview of the deformation and fracture behavior of different classes of materials, including (**a**) ductile materials (Hirth and Lothe 1982), (**b**) brittle materials (Broberg 1990) and (**c**) BPMs (Buehler and Ackbarow 2007). Each subplot shows a multi-scale view of associated deformation mechanisms. In ductile materials, deformation is mediated by creation of dislocation networks; each dislocation represents localized shear of an atomic lattice. In brittle materials, fracture occurs by spreading of cracks, which is mediated by continuous breaking of atomic bonds. In BPMs, a complex interplay of different protein structures controls the mechanical response. At the ultra-scale, unfolding of individual protein molecules by rupture of hydrogen bonds (HBs) represents the most fundamental deformation mechanism

For example, ductile metals such as copper or nickel can rather easily undergo large permanent (or "plastic") deformation without breaking (Hirth and Lothe 1982). On the other hand, brittle materials like glass cannot easily be deformed, but instead fracture rapidly once the applied load exceeds a threshold value (Broberg 1990). Contrarily, biological protein materials (BPMs) such as the cell's cytoskeleton or collagen networks in tendon or bone represent intriguing protein networks that can dynamically adapt to load application by self-organization and self-arrangement; developing stronger filaments when needed and disposing of those that do not contribute to the strength, making the material utilization overall more efficient and robust against failure.

Advancing the understanding of the origin of deformation and fracture has fascinated generations of material scientists. Currently, a major challenge is the elucidation of mechanisms in increasingly complex materials – materials that consist of multiple components or multiple hierarchies, or those whose atomic nanostructures and microstructures contain a concurrent interplay of a variety of chemical bonds. An important concept in understanding the deformation and failure properties of materials are the underlying fundamental atomic mechanisms, as illustrated in Fig. 8.2 for ductile materials, brittle materials and BPMs (Buehler and Ackbarow 2007) (see caption of Fig. 8.2 for an overview of the various deformation modes). While the basic deformation mechanisms of crystalline solids are relatively well understood, analogous mechanisms have only recently been discovered in BPMs. Permanent plastic deformation in these materials is mediated by intermolecular slip, unfolding of proteins (Rief et al. 1997; Lu et al. 1998; Buehler and Ackbarow 2007), breaking of intermolecular cross-links or stretching of convoluted protein chains, as it has for instance been demonstrated in multi-scale studies for collagenous materials and bone.

Due to the multi-scale hierarchical structure of these materials, different deformation mechanisms may occur at each scale, while the inter- and intra-hierarchal interactions might be of competing or of reinforcing character. The most fundamental deformation mode is often, however, breaking of weak bonds, for instance the rupture of individual H-bonds (HBs). Even though they are 100–1,000 times weaker than covalent bonds, HBs are the most important type of chemical bonds that hold together proteins, assemblies of proteins and control their adhesion behavior. An important open question thereby is how weak interactions can be utilized to make up macroscopically strong materials. Up until now, few systematic classifications, nor fundamental theories exist for the different deformation and fracture mechanisms in BPM.

### *8.1.2 Collagen Structure – From Atoms to Tissue*

Collagen consists of tropocollagen molecules that have lengths of $L \approx 300$nm with approximately 1.5 nm in diameter, leading to an aspect ratio of close to 200 (Ramachandran and Kartha 1955; Bhattacharjee and Bansal 2005). Staggered arrays

of tropocollagen molecules form fibrils, which arrange to form collagen fibers. A schematic of the main hierarchical features of collagen is shown in Fig. 8.3.

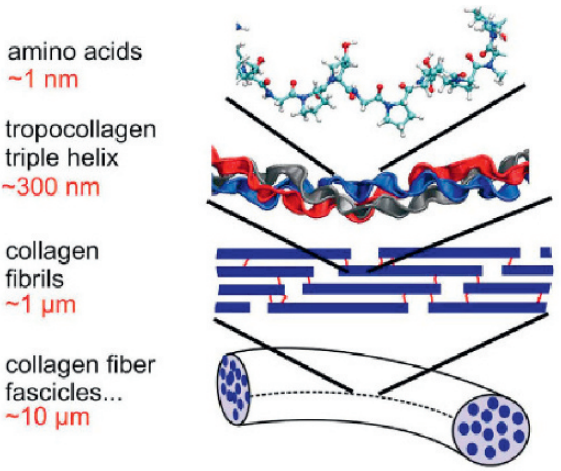


**Fig. 8.3** Schematic view of some of the hierarchical features of collagen, ranging from the amino acid sequence level at nanoscale up to the scale of collagen fibers with lengths on the order of 10 µm (Figure adapted from Buehler 2006a,b). The present study is focused on the mechanical properties of collagen fibrils, consisting of a staggered array of TC molecules. The red lines in the graph indicate intermolecular cross-links that are primarily developed at the ends of tropocollagen molecules

Each tropocollagen molecule consists of a spatial arrangement of three polypeptides. These three molecules or polypeptides are arranged in a helical structure, stabilized primarily by H-bonding between different residues. Every third residue in each of these molecules is a GLY amino acid, and about one-fourth of the tropocollagen molecule consists of proline (PRO) and hydroxyproline (HYP). The structure of collagen has been known since classical works focusing on theoretical understanding of how tropocollagen molecules are stabilized (Ramachandran and Kartha 1955; Bhattacharjee and Bansal 2005). Recently, various types of tropocollagen molecules have been crystallized and analyzed using X-ray diffraction techniques to determine their precise atomic configuration (Kramer et al. 2000). TEM experiments have also been used to study the structure of collagen in various environments, including in bone, in particular focusing on larger length scale features and its three-dimensional arrangement (Weiner and Wagner 1998; Currey 2002; Ritchie et al. 2004; Nalla et al. 2005).

Collagen is the most fundamental building block of bone, providing additional evidence for the great significance of collagen. Bone has evolved to provide structural support to organisms, and therefore, its mechanical properties are of great physiological relevance. A total of seven hierarchical levels are found in bone. The smallest scale hierarchical features of bone include the protein phase composed of tropocollagen molecules, collagen fibrils (CFs) as well as mineralized collagen fibrils (MCFs). Tropocollagen molecules assemble into collagen fibrils in a hydrated environment, which mineralizes by formation of hydroxyapatite (HA) crystals in the gap regions that exist due to the staggered geometry (Laudis et al. 2002; Currey 2002; Weiner and Wagner 1998).

### *8.1.3 Outline of This Chapter*

The analysis reported in this chapter is focused on molecular and supermolecular deformation mechanisms as well as prevalent molecular length scales in collagenous tissues. The results help to explain the particular molecular architecture as observed in tendon, bone and the eye's cornea, and provide models that predict how molecular properties influence the deformation and fracture mechanics of tissues. This chapter consists of seven sections that are dedicated to a review of atomistic and molecular simulation techniques, geared toward improving our understanding of the mechanical behavior of collagenous tissue, at the atomistic, molecular and supermolecular scales. It is noted that while this chapter includes a review of the broader field, the focus is on results from our group.

In Section 8.2, we discuss the numerical foundation and theoretical framework of the analysis techniques reviewed in this chapter, in particular atomistic simulation approaches. The subsequent sections systematically discuss various scales of collagen, ranging up to the scale of mineralized collagen fibrils. Section 8.3 is dedicated to atomistic simulations of individual tropocollagen molecules. This section also includes an analysis of the interaction between two tropocollagen molecules. In Section 8.4, the mechanical behavior of collagen fibrils is discussed, including studies of effects of the molecular length and cross-link densities. In Section 8.5, we review studies of mineralized collagen fibrils, forming the fundamental building block of bone. Section 8.6 is dedicated to a broader discussion on structure–function relationships of hierarchical biological materials. We conclude in Section 8.7 with a discussion.

## 8.2 Numerical Simulation Techniques and Theoretical Framework

In order to develop a fundamental and quantitative understanding of collagen mechanics, theoretical models encompassing the mesoscopic scales between the atomistic and the macroscopic levels, considering atomistic and chemical interactions during deformation, are vital. This represents an alternative strategy capable of predicting the properties of collagen tissue from bottom up.

In order to achieve this goal, a parameter-free atomistic-based model of the mechanical properties of collagen fibrils, based solely on atomistic simulation input data, can be used (Buehler 2006a, b, Buehler 2008).

Materials failure processes begin with the erratic motion of individual atoms around flaws or defects within the material that evolve into formation of macroscopic fractures as chemical bonds rupture rapidly, eventually compromising the integrity of the entire structure. Thus the behavior of chemical bonds under large stretch – on a small scale – controls how structures respond to mechanical load and fail on much larger material scales, as has for instance been demonstrated by our group for model materials and silicon (Buehler et al. 2003; Buehler et al. 2006; Buehler and Gao 2006; Buehler et al. 2007).

Fracture mechanisms in brittle and ductile materials are representative examples for an intrinsic multi-scale problem that cannot be understood by considering one scale alone (see Figs. 8.1 and 8.2). Experimentation, simulation and development of theories therefore must consider a complex interplay of mechanisms at several scales. In particular in hierarchical BPMs, development of a rigorous understanding of deformation depends critically on the elucidation of the deformation mechanism at each scale and on how these mechanisms interact dynamically, across the scales. These examples illustrate the importance of developing fundamental, atomistic or molecular scale models of the behavior of collagenous tissues.

### *8.2.1 Multi-scale Modeling of Deformation and Failure*

Multi-scale modeling is a particularly useful approach to gain insight into complex deformation and fracture phenomena. In order to allow the best resolution at any length and time scale, a set of computational methods is integrated seamlessly, which enables one to bridge scales from nano to macro (see Fig. 8.4).

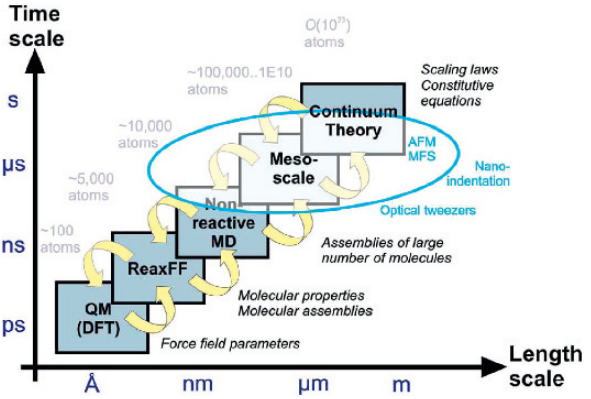


**Fig. 8.4** Schematic that illustrates the concept of hierarchical multi-scale modeling (Figure adapted from (Buehler and Ackbarow 2007)). Hierarchical coupling of different computational tools can be used to traverse throughout a wide range of length and time scales. Such methods enable to provide a fundamental insight into deformation and fracture phenomena, across various time and length scales. Handshaking between different methods enables one to transport information from one scale to another. Eventually, results of atomistic, molecular or mesoscale simulation may feed into constitutive equations or continuum models. While continuum mechanical theories have been very successful for crystalline materials, BPMs require statistical theories, e.g., the Extended Bell Model (Ackbarow et al. 2007; Ackbarow and Buehler 2007b). Experimental techniques such as atomic force microscope (AFM), molecular force spectroscopy (MFS), nanoindentation or optical tweezers now overlap into atomistic and molecular approaches, enabling direct comparison of experiment and simulation (Lim et al. 2006)

Atomistic simulation, or molecular dynamics (MD) (Allen and Tildesley 1989), provides one with a fundamental view on materials deformation – describing the patterns of fracture, yield, diffusion and other mechanisms at resolutions that cannot yet

be reached by experiments. After careful validation of these computational models with experiments, atomistic and multi-scale modeling has predictive power. Predictive multi-scale simulation could play an important role in science, engineering and materials design in the coming decades.

### 8.2.2 Basics of Atomistic Modeling

The basic concept behind atomistic simulation via MD is to calculate the dynamical trajectory of each atom in the material, by considering their atomic interaction potentials, by solving each atom's equation of motion according to $F = ma$. Numerical integration of this equation by considering proper interatomic potentials enables one to simulate a large ensemble of atoms that represents a larger material volume, albeit typically limited to several nanoseconds of time scale. The availability of such potentials for a specific material is often a limiting factor in applicability of this method.

Classical molecular dynamics generates the trajectories of a large number of particles, interacting with a specific interatomic potential, leading to positions $r_i(t)$, velocities $v_i(t)$ and accelerations $a_i(t)$. It can be considered an alternative to methods like Monte Carlo, with the difference that MD actually provides full dynamical information – and deterministic trajectories. The total energy of the system ($E$) is written as the sum of kinetic energy ($K$) and potential energy ($U$),

$$E = K + U, \tag{8.1}$$

where the kinetic energy is

$$K = \frac{1}{2} m \sum_{j=1}^{N} v_j^2, \tag{8.2}$$

and the potential energy is a function of the atomic coordinates $r_j$,

$$U = U(r_j), \tag{8.3}$$

with a properly defined potential energy surface $U(r)$, where $r = \{r_i\}$ describes the set of all atomic coordinates in the system. The numerical problem to be solved is a system of coupled second-order nonlinear differential equations:

$$m \frac{\mathrm{d}^2 r_j}{\mathrm{d}t^2} = -\nabla_{r_j} U(r) \quad j = 1 \ldots N, \tag{8.4}$$

which can only be solved numerically for more than two particles, $N > 2$. Typically, MD is based on updating schemes that yield new positions from the old positions, velocities and the current accelerations of particles:

$$r_i(t_0 + \Delta t) = -r_i(t_0 - \Delta t) + 2r_i(t_0)\Delta t + a_i(t_0)(\Delta t)^2 + \cdots. \tag{8.5}$$

The forces and accelerations are related by $a_i = f_i/m$. The forces are obtained from the potential energy surface – sometimes also called force field – as

$$F = m\frac{\mathrm{d}^2 r_j}{\mathrm{d}t^2} = -\nabla_{r_j} U(r) \quad j = 1 \ldots N. \tag{8.6}$$

This technique can not only be used for particles that are atoms, but also be applied for particles that represent groups of atoms, such as in bead models. Provided interatomic potentials are available, MD is capable of directly simulating a variety of materials phenomena, for instance the response of an atomic lattice to applied loading under the presence of a crack-like defect, or the unfolding mechanisms of proteins.

One of the strengths of atomistic methods is its very fundamental viewpoint of materials phenomena. The only physical law that is put into the simulations is Newton's law and a definition of how atoms interact with each other. Despite this very simple basis, very complex phenomena can be simulated. Unlike many continuum mechanics approaches, atomistic techniques require no a priori assumption on the defect dynamics. A drawback of atomistic simulations is the difficulty of analyzing results and the large computational resources necessary to perform the simulations. Once the atomic interactions are chosen, the complete material behavior is determined. Different interatomic potentials are used in the studies of collagen at different scales; specific methods and theories will be introduced in the subsequent sections.

### *8.2.3 Large-Scale Parallelized Computing*

Large-scale molecular dynamics simulations often require a significant amount of computing resources. Classical molecular dynamics can be quite efficiently implemented on modern supercomputers using parallelized computing strategies. Such supercomputers are composed of hundreds of individual computers (see, e.g. www.top500.org).

We now expect petaflop computers by the middle or end of the current decade. Based on the concept of concurrent computing, modern parallel computers are made out of hundreds or thousands of small computers working simultaneously on different parts of the same problem. Information between these small computers is shared by communicating, which is achieved by message passing procedures, enabled via software libraries such as the "Message Passing Interface" (MPI) (Gropp et al. 1999; Kadau et al. 2004).

Implemented based on spatial domain decomposition, parallel MD reaches linear scaling, that is the total execution time scales linear with the number of particles $\sim N$, and scales inversely proportional with the number of processors used to solve the numerical problem, $\sim 1/P$ (where $P$ is the number of processors).

With a parallel computer whose number of processors increases with the number of cells (the number of particles per cell does not change), the computational burden remains constant. To achieve this, the computational space is divided into cells such that in searching for neighbors interacting with a given particle, only the cell in which it is located and the next-nearest neighbors have to considered. This scheme allows to treat huge systems with several billion particles.

### *8.2.4 Analysis and Visualization*

A versatile, powerful and widely used visualization tool is the visual molecular dynamics (VMD) program (Humphrey et al. 1996). This software enables one to render complex molecular geometries using particular coloring schemes. It also enables us to highlight important structural features of proteins by using a simple graphical representation, such as alpha-helices, or the protein's backbone. The simple graphical representation is often referred to as cartoon model. In this particular cartoon model, the triple-helical structure of the tropocollagen motif is clearly visible. This is shown in Fig. 8.5.

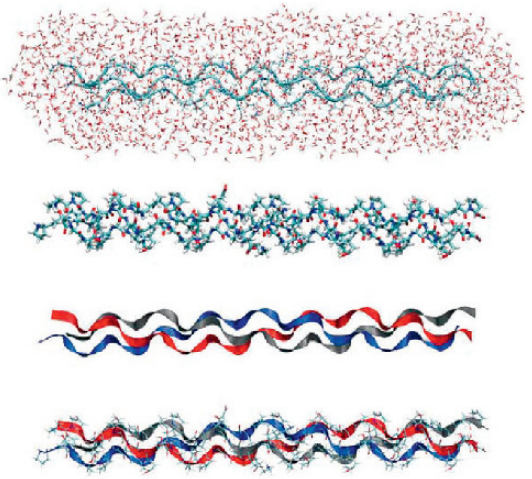

**Fig. 8.5** Different representation of a single tropocollagen molecule, realized by the visualization program VMD (Humphrey et al. 1996). The upper plot shows the TC molecule solvated in water, the second plot from the top shows a tropocollagen molecule without the water molecules and the lower parts show a cartoon representation of the molecular geometry. In each subplot, the same molecular structure is visualized, illustrating the potential of visualization methods

An important quantity in the analysis of mechanical properties is the Cauchy stress tensor. For most studies discussed here we use the virial stress to calculate the Cauchy stress tensor directly from atomistic data (Tsai 1979; Zimmerman et al. 2004). The atomistic data is averaged over all particles (spatial average) and over several snapshots (temporal average). The virial stress is calculated by considering the volume of the computational sample, including the free volume in the molecular structure. For details regarding the calculation of the virial stress tensor we refer the reader to the literature (Tsai 1979; Zimmerman et al. 2004).

Energy dissipation per unit volume is calculated by integrating over the stress–strain curve until the fibril has fractured (strain $\varepsilon_F$), according to

$$E_{\text{diss},V} = \int_{\tilde{\varepsilon}=0}^{\varepsilon_F} \sigma(\tilde{\varepsilon}) \mathrm{d}\tilde{\varepsilon}. \tag{8.7}$$

### 8.2.5 Complementary Experimental Methods

Recent advances in experimental techniques further facilitate analyses of ultra-small-scale material behavior. For instance, techniques such as nanoindentation, optical tweezers or atomic force microscopy (AFM) can provide valuable insight to analyze the molecular mechanisms in a variety of materials, including metals, ceramics and proteins. A selection of experimental techniques is summarized in Fig. 8.4, illustrating the overlap with multi-scale simulation methods.

An important experimental technique in conjunction with atomistic modeling of protein materials is X-ray diffraction; results of such experiments provide the initial atomistic and molecular structure, the starting point for all atomistic simulations. The structure of many proteins, elucidated using such experiments, has been deposited in the Protein Data Bank (PDB).

### 8.2.6 Summary

In this section, we have summarized the key aspects of molecular modeling, including basic molecular dynamics, a brief discussion on supercomputing as well as a brief review of complementary experimental methods.

## 8.3 Deformation and Fracture of Single Tropocollagen Molecules

This section is focused on the nanomechanical properties of single tropocollagen molecules, as originally reported in (Buehler 2006a, b; Buehler and Wong 2007). This approach in describing collagenous tissues represents a bottom-up approach, focusing on the finest, atomistic scales of detail governed by quantum mechanics (QM) as starting point, reaching up to large, macroscopic scales, using hierarchical multi-scale modeling. The first step in achieving this goal is the careful study of the properties of a single molecule.

There are several reports of experimental studies focused on the mechanics of single tropocollagen molecules (Waite et al. 1998; Arnoux et al. 2002; Sun et al. 2002; An et al. 2004). However, despite its relatively simple structure (for a recently crystallized model protein please see Kramer et al. 2000), single tropocollagen molecules have rarely been studied using molecular dynamics (MD) studies. In one of the few reports found in the literature, Lorenzo and coworkers (Lorenzo and Caffarena 2005) have reported investigations of the mechanical

properties of collagen fibers, using MD studies, focusing on their Young's modulus. Other studies focused on the stability of collagen molecules (Israelowitz et al. 2005) and other structural investigations (Mooney et al. 2001; Mooney and Klein 2002; Mooney et al. 2002), or the effect of point mutations on the stability (Israelowitz et al. 2005). Some researchers modeled collagen at the continuum scale, using techniques such as the Finite Element Method (Bischoff et al. 2000).

Questions of particular interest include: How does a tropocollagen molecule respond to mechanical stretching force, in particular at large stretches? How does it fracture? How can these properties be linked to the folded structure? How do ultra-long collagen molecules with realistic lengths of several hundred nanometers behave in solution, under mechanical stretch? Such insight is important to understand the role of individual tropocollagen molecules in the context of tissue mechanics.

After a brief review of our computational technique in Section 8.3.1, we report atomistic modeling of the mechanics of single collagen fibers under different types of loading in Section 8.3.2. In Section 8.3.3 we provide a discussion of the results.

Table 8.1 provides an overview of important mathematical symbols used throughout this chapter.

### *8.3.1 Atomistic Model*

Definition of the atomic interactions by force fields is at the heart of MD methods, as it defines the complete materials behavior. The basis for our investigations is a combination of the classical CHARMM force field (MacKerell et al. 2000) and the ReaxFF reactive force field (Duin et al. 2001; Strachan et al. 2005). The CHARMM

**Table 8.1** Description of the main parameters and material or molecular properties used in the manuscript. Units are provided for some of the variables

| | |
|---|---|
| $F_{\text{tens}}$ | Tensile strength of a bimolecular fibril (geometry see Fig. 8.23) |
| $A_{\text{C}}$ | Cross-sectional area of a TC molecule |
| $L_0$ | Length of an individual TC molecule |
| $L$ | Length of a TC molecule in a collagen fibril |
| $L_{\text{C}}$ | Contact length between different TC molecules (e.g., in a bimolecular assembly or in a collagen fibril) |
| $\alpha$ | Overlap parameter in an assembly of TC molecules, note that $\alpha = L_{\text{C}}/L$ |
| $\tau_{\text{shear}}$ | Shear strength between two TC molecules (units: force/length) |
| $\sigma_{\text{R}}$ | Critical molecular tensile stress to nucleate slip pulse |
| $E$ | Young's modulus, e.g., of an individual TC molecule or a collagen fibril |
| $\sigma_{\text{tens}}$ | Tensile stress in a TC molecule (note that $\sigma_{\text{tens}} = F_{\text{tens}}/A_{\text{c}}$) |
| $F_{\text{max}}$ | Maximum tensile force a single TC molecule can sustain |
| $F_{\text{F}}$ | Maximum tensile force a BM collagen fibril can sustain |
| $\chi_{\text{S}}$ | Critical molecular length scale beyond which slip pulse nucleation occurs |
| $\chi_{\text{R}}$ | Critical molecular length scale beyond which fracture occurs |
| $L_\chi$ | Critical molecular length scale at which maximum strength is reached |
| $\gamma$ | Energetic barrier to nucleation of a slip pulse (units: energy per length$^2$) |
| $E_{\text{diss}}$ | Energy dissipation during deformation (units: energy) |
| $E_{\text{diss,V}}$ | Energy density dissipation during deformation (units: energy per volume) |

model is a widely used model to describe the behavior of proteins and related materials and structures.

However, for extreme mechanical loading and large deformation close to the breaking point, such classical approaches fail and new methods are required that take into consideration the behavior of chemical bonds at large deformation. We employ a new generation of reactive force fields to account for these chemical effects in protein mechanics.

#### 8.3.1.1 Classical CHARMM Force Field

The classical force field CHARMM, implemented in the MD program NAMD (Nelson et al. 1996; MacKerell et al. 1998), is used for deformation studies of tropocollagen molecules and assemblies of tropocollagen molecules. The CHARMM force field (Anderson 2005) is widely applied in the protein and biophysics community and provides a basic description of proteins. It is based on harmonic and anharmonic terms describing covalent interactions, in addition to long-range contributions describing van der Waals (vdW) interactions, ionic (Coulomb) interactions, as well as hydrogen bonding. Since the bonds between atoms are modeled by harmonic springs or its variations, bonds between atoms cannot be broken and new bonds cannot be formed. Also, the charges are fixed and cannot change, and the equilibrium angles do not change depending on stretch. We have added an extension to the standard CHARMM force field to include a description of the hydroxyproline residue ("HYP" in the PDB file), which is not one of the 20 natural amino acids, following the procedure suggested in Anderson (2005).

#### 8.3.1.2 Reactive Force Field: A New Bridge to Integrate Chemistry and Mechanics

Reactive force fields represent an important milestone in overcoming the limitations of classical force fields in not being able to describe chemical reactions. For mechanical properties, this translates into the properties of molecules at large strain, a phenomenon referred to as hyperelasticity. Several flavors of reactive potentials have been proposed in recent years (Stuart et al. 2000; Duin et al. 2001; Brenner et al. 2002). Reactive potentials can overcome the limitations of empirical force fields and enable large-scale simulations of thousands of atoms with quantum mechanics accuracy. The reactive potentials, originally only developed for hydrocarbons (Duin et al. 2003; Strachan et al. 2003; van Duin et al. 2004; Chenoweth et al. 2005; Cheung et al. 2005; Han et al. 2005; Nielson et al. 2005; Strachan et al. 2005; Buehler et al. 2006; Buehler 2007; Buehler et al. 2007), have been extended recently to cover a wide range of materials, including metals, semiconductors and organic chemistry in biological systems such as proteins. Here we employ a particular flavor of the ReaxFF potentials as suggested in Datta et al. (2005), with slight modifications to include additional QM data suitable for protein modeling.

Reactive potentials are based on a more sophisticated formulation than most nonreactive potentials. A bond length/bond order relationship is used to obtain smooth transition from non-bonded to single-, double- and triple-bonded systems.

All connectivity-dependent interactions (that means, valence and torsion angles) are formulated to be bond order dependent. This ensures that their energy contributions disappear upon bond dissociation so that no energy discontinuities appear during reactions. The reactive potential also features non-bonded interactions (shielded van der Waals and shielded Coulomb).

The reactive formulation uses a geometry-dependent charge calculation (QEq) scheme similar to Goddard's QEq (Rappé and Goddard 1991) that accounts for polarization effects and modeling of charge flow. This is a critical advance leading to a new bridge between QM and empirical force fields. All interactions feature a finite cutoff. Figure 8.6 shows a comparison between reactive and nonreactive formulations, illustrating that both descriptions agree for small deviations from the equilibrium, but disagree significantly for large strains.

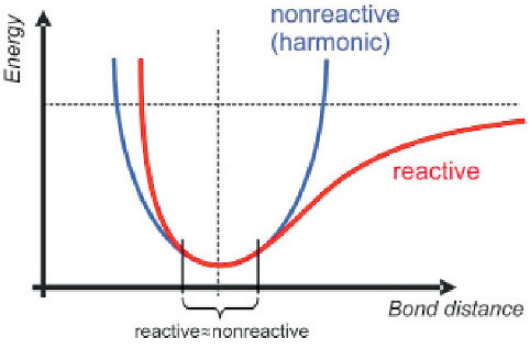


**Fig. 8.6** Schematic illustration of the differences between a reactive and nonreactive force field. The schematic illustrates that the nonreactive model is only valid for small deformation from the equilibrium bond configuration and cannot describe dissociation of the chemical bond. The reactive description overcomes these limitations (for further information, see for instance Buehler 2007)

### 8.3.1.3 Preprocessing

Preprocessing of the simulations is done using the CMDF framework (Buehler and Dodson et al. 2006), a computational Python-based simulation environment capable of seamless integration of various file formats, computational engines, including molecular and crystal building tools.

Python scripts are used to analyze and post-process the simulation data, as required for example to compute statistical averages of force–displacement curves.

### 8.3.1.4 Atomistic Simulation Procedure

We build the atomistic based on the crystal unit cells according to X-ray diffraction data obtained by experiment; a short tropocollagen segment is solvated in a water skin. These structures are taken directly from the Protein Data Bank (PDB). We use the crystal structure PDB ID 1QSU, with 1.75 Å resolution, as reported by Kramer and coworkers (Kramer et al. 2000). The 1QSU is a triple-helical collagen-like

molecule with the sequence (Pro-Hyp-Gly)$_4$-Glu-Lys-Gly-(Pro-Hyp-Gly)$_5$ (structure is also shown in Fig. 8.5 in various visualization modes).

The charges of each atom are assigned according to the CHARMM rules. Hydrogen atoms are added according to pH 7. The CHARMM input files (structure and topology files) are then used to perform NAMD calculations. For ReaxFF calculations, no atom typing is necessary (only element types are assigned), and charges are determined dynamically during the simulation. Hydrogen atoms are added using the NAMD/CHARMM procedure, according to the same conditions as outlined above.

Before finite temperature, dynamical calculations are performed; we carry out an energy minimization, making sure that convergence is achieved, thus relieving any potential overlap in vdW interactions after adding hydrogen atoms. In the second step, we anneal the molecule after heating it up to a temperature $T = 300\,\mathrm{K}$. The heat up rate is $\Delta T = 25\,\mathrm{K}$ every 25 steps, and we keep the temperature fixed after the final temperature $T = 300\,\mathrm{K}$ is achieved (then we apply a temperature control in an NVT ensemble). We also ensure that the energy remains constant after the annealing procedure. The relaxed initial length of each molecule (consisting of 30 residues in each of the three chains) is $L_0 = 84\,\text{Å}$.

Depending on the details of the loading case, we then apply mechanical forces using varied types of constraints and investigate the response of the molecule due to the applied loading. Typically, we obtain force-versus-displacement data, which are then used to extract mechanical quantities such as stress and strain, using continuum mechanical concepts by drawing analogies between the molecular level and continuum mechanical theories. Steered MD is based on the concept of adding restraint force to groups of atoms by extending the Hamiltonian by an additional restraint potential of the form $1/2\,k_{\mathrm{SMD}}(r - r_\lambda)^2$. The SMD method mimics a AFM nanomechanics experiment, as illustrated in Fig. 8.7.

Unless indicated otherwise, we use a steered molecular dynamics (SMD) scheme with spring constant $k_{\mathrm{SMD}} = 10\,\mathrm{kcal/mol/Å}^2$. It was shown in previous studies that this is a reasonable choice leading to independence of the measured molecular mechanical properties from the choice of the SMD spring constant (Lorenzo and Caffarena 2005).

#### 8.3.1.5 Computational Experiments of Stretching Short Tropocollagen Segments

In the following section, we present a suite of studies with different mechanical loading. The different loading cases studied in this chapter are summarized in Fig. 8.8. The different loading conditions and the objective of the specific calculation are:

- Tensile/compressive testing (obtain Young's modulus/buckling load), Fig. 8.8(a)
- Bending (obtain bending stiffness and persistence length), Fig. 8.8(b)
- Shearing two tropocollagen molecules (obtain fiber–fiber interactions), Fig. 8.8(c)

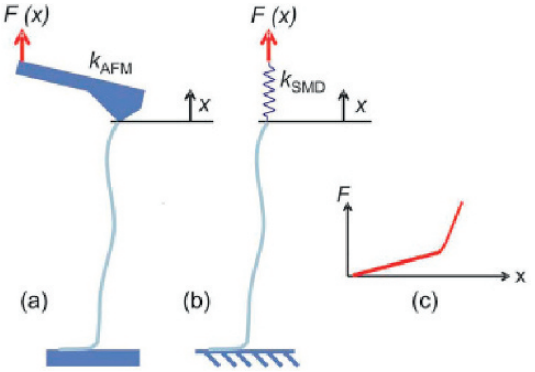


**Fig. 8.7** Single molecule pulling experiments, carried out on a single protein molecule (Buehler and Ackbarow 2007). Subplot (**a**) depicts an experimental setup based on AFM and subplot (**b**) depicts a steered molecular dynamics (SMD) analogue. In the SMD approach, the end of the molecule is slowly pulled at a pulling velocity $v$ vector. This leads to a slowly increasing force $F = k(v \cdot t - x)$ ($k = 10\,\text{kcal/mol/Å}^2$), where $t$ is the time and $x$ is the current position vector of the end of the molecule ($F(x)$, schematically shown in subplot (**c**)). Both approaches, AFM and SMD, lead to force–displacement information. In addition to the $F(x)$ curve, SMD provides detailed information about associated atomistic deformation mechanisms. Due to the time scale limitations of MD to several nanoseconds, there is typically a large difference between simulation and experiment with respect to pulling rates. Whereas MD simulations are limited to pulling rates of $\approx 0.01\,\text{m/s}$, experimental rates are six to eight magnitudes smaller than those. This requires additional consideration in order to interpret MD results in light of experimental findings

## *8.3.2 Tensile and Compressive Loading*

### 8.3.2.1 Small Deformation

First we discuss tensile testing of the fibers using the nonreactive CHARMM force field. After careful equilibrium of the structure of the collagen molecule, we apply a force at one end, while we keep the other end of the molecule fixed. The loading case is shown in Fig. 8.8(a). By slowly increasing the load applied to the collagen

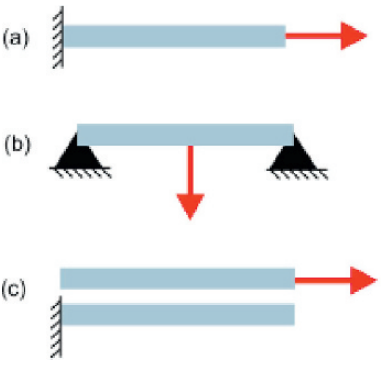


**Fig. 8.8** Overview of various load cases studied, as reported in Buehler (2006a,b). Our load cases include (**a**) tensile loading in axial direction of the molecule (also including compressive test), (**b**) bending test and (**c**) shear test

molecule, while measuring the displacement $d$, we compute force–displacement curves. The force-versus-displacement curve $F(d)$ can be used to determine a stress versus strain curve, by proper normalization:

$$\sigma(d) = \frac{F(d)}{A_C}, \tag{8.8}$$

where $A_C$ denotes an equivalent area of the cross-section of a collagen molecule, and $A_C = \pi \cdot R^2 \approx 214.34\,\text{Å}^2$, assuming that $R = 8.26\,\text{Å}$ (obtained from studies of an assembly of two tropocollagen molecule as described below). Note that the stress is typically dependent on the stretch $d$. The local (in terms of strain) Young's modulus $E(d)$ is given by

$$E(d) = \frac{d_0}{A_C}\frac{\partial F(d)}{\partial d}, \tag{8.9}$$

where $d_0$ is the initial, undeformed length of the collagen fiber and $d_0 = 84\,\text{Å}$. Note that Young's modulus is independent of the length of the molecule. The definition in Eq. (8.9) is a consequence of the fact that the stretching force is expressed as a function of stretch $d$ rather than strain ($\sigma = E\varepsilon$).

Figure 8.9 shows force-versus-displacement plots for tensile loading, for three different loading rates. The loading rates in the three cases are $\dot{r}_\lambda = 0.0001$, 0.0002 and 0.001 Å/step, respectively. Young's modulus is determined as the tangential slope corresponding to 10% tensile strain. Young's modulus is obtained to be $E_{\text{tens}} = 6.99$, 8.71 and 18.82 GPa, respectively, for increasing loading rates as specified above. We observe an increase in stiffness for higher loading rates. These results indicate that collagen fibers show a rate-dependent elastic response.

The estimate for Young's modulus is somewhat in agreement with results reported in Lorenzo and Caffarena (2005), presenting a value for Young's modulus

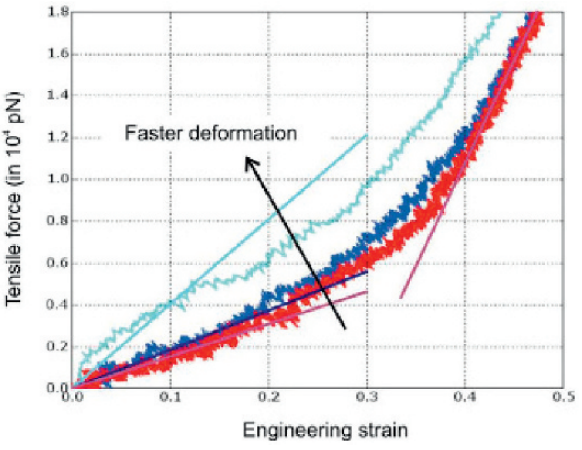


**Fig. 8.9** Force versus strain, pulling of a single tropocollagen molecule, for three different pulling velocities, as reported in Buehler (2006a). The results indicate that faster pulling velocities lead to a stiffening effect (the loading rates in the three cases are $\dot{r}_\lambda = 0.0001$, 0.0002 and 0.001 Å/step, respectively)

of around $4.8 \pm 1.0$ GPa. The reason for the difference to our results could be the different force field used, different boundary conditions or different strain rates.

Figure 8.10 depicts snapshots of the tropocollagen molecule under increasing stretch. At large strains, the helical structure is lost and the three polypeptides appear as individual strands, then defining its elasticity by the behavior of covalent bonds. This is also confirmed in the force–strain plot (Fig. 8.9). The "local" Young's modulus associated with large strains is given by $E_{\text{tens}}^{\text{large}} = 46.7$ GPa.

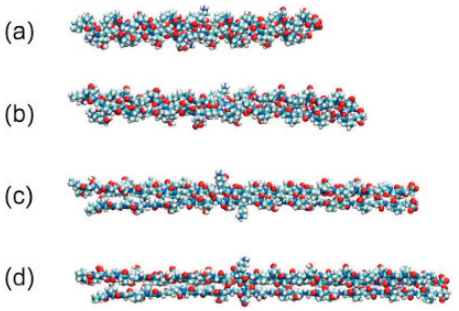


**Fig. 8.10** Stretching of a single tropocollagen molecule, using a nonreactive CHARMM force field (water molecules are not shown for clarity) (Buehler 2006). The helical structure unfolds with increasing strain and vanishes at large deformation and the three strands become independent and the covalent bonds between atoms govern the elasticity. This loss in tertiary helical structure is represented by a change in tangent elasticity, as seen in Fig. 8.9, at strains beyond 35%

Under compressive loading, it is observed that the tropocollagen molecule can only sustain a relatively small load before buckling. Figure 8.11 shows load versus displacement curves, and Fig. 8.12 depicts several snapshots as the collagen molecule is subjected to compressive loading. The maximum force level sustained before buckling is $F_{\text{max,compr}} \approx 1,050$ pN, reached at about 5% compressive strain. Young's modulus under compressive loading, calculated for very small strains

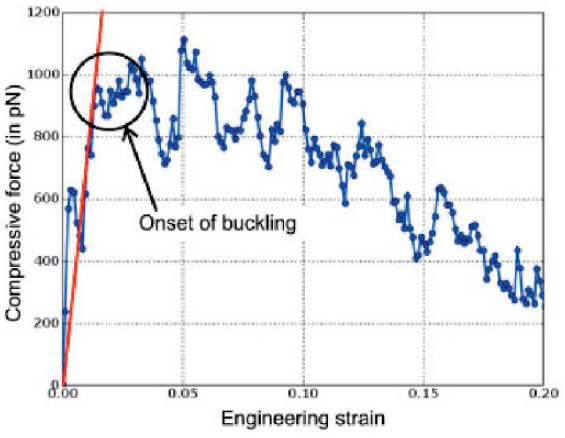


**Fig. 8.11** Compressive loading of the single tropocollagen molecule, at a loading rate of $\dot{r}_\lambda = 0.0002$ Å/step (Buehler 2006a). The behavior under compression is significantly different than under tension, also revealing an asymmetry of the elastic properties at small strains. The tropocollagen molecule starts to buckle at about 5% compressive strain

up to 1.25%, is given by $E_{\text{compr}} \approx 29.86\,\text{GPa}$. This indicates that the elastic tensile/compressive behavior is asymmetric around the equilibrium position, with significantly higher compressive modulus than tensile modulus. However, the maximum load that can be sustained under pure compression is much lower than under tension due to buckling.

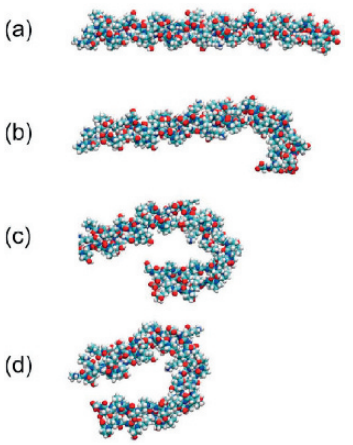


**Fig. 8.12** Tropocollagen molecule under compressive loading (water molecules are not shown for clarity) (Buehler 2006a). The results suggest that upon a relatively small load, the tropocollagen molecule starts to buckle and goes into a bending mode

#### 8.3.2.2 Large Deformation and Fracture Mechanics of Individual Tropocollagen Molecules

Now we focus on the mechanical behavior of tropocollagen molecules using a reactive force field. The dominating forces in tropocollagen molecules occur typically in the axial direction of the molecule, so this type of loading is most critical for the mechanical integrity of tissues.

Questions that we would like to investigate include: Under which conditions do classical, nonreactive force fields break down, and what are the limitations of these methods? Do the results agree for small deformation? How are the mechanical properties different once mechanical deformation is large and formation and breaking of bonds are allowed? We will pull the tropocollagen molecule until fracture occurs and study the details of the fracture mechanisms. A central question we would like to address is, to which strain and deformation levels – or, equivalently, applied force level – can we rely on the assumption of nonreactive force fields. A solid understanding of the large deformation, nonlinear and fracture properties of tropocollagen molecules becomes important when the mesoscale model is introduced at the next hierarchical level.

Figure 8.13 depicts snapshots of results obtained from ReaxFF simulations of tensile deformation of tropocollagen molecules. We observe that the shape of the fiber changes from a straight shape to an S-like shape as the load increases. This change of shape leads to an increasingly large radius of curvature in localized regions of the fiber (toward the left and right ends). These regions with high

curvature represent regions of higher tensile stress. In agreement with this notion, we observe that these regions lead to onset of failure. A possible explanation for the transformation into the S-like shape may be the different energy expression in the reactive potential. The change of bond behavior at large deformation is not linear, but instead, it is nonlinear, eventually leading to rupture of covalent bonds.

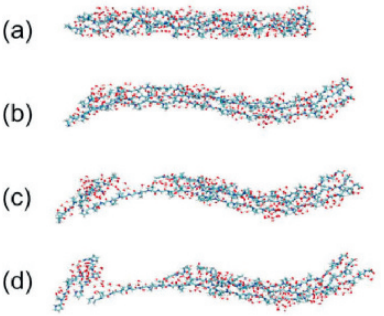


**Fig. 8.13** Fracture mechanics of a single tropocollagen molecule, as reported in Buehler (2006a). We observe a transformation from the initial straight shape to an S-shaped structure at large strain, leading to fracture of an individual polypeptide. This transformation is found consistently for a variety of loading conditions

Figure 8.14 shows plots of force versus strain, comparing the CHARMM model (curve (a)) with the ReaxFF model (curve (b)). The strength of the tropocollagen molecule is determined to be $2.35 \times 10^4$ pN, reached at approximately 50% tensile strain. We find that the CHARMM description and the ReaxFF model agree for

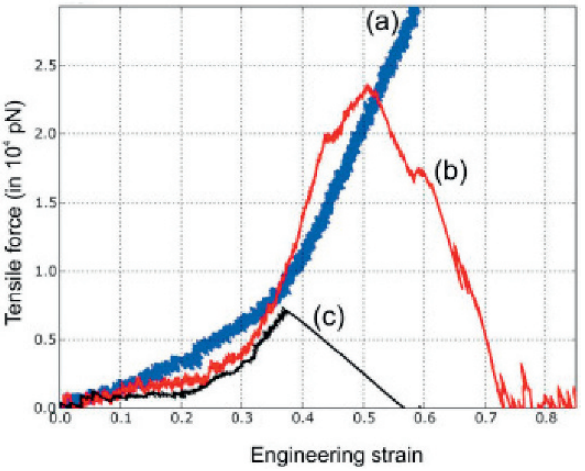


**Fig. 8.14** Force versus strain, pulling of a single tropocollagen molecule, as reported in Buehler (2006a). An initial regime of flat, almost linear elastic extension is followed by onset of nonlinear, stiffening behavior at larger strains beyond approximately 30–35% strain. This behavior can be explained by the fact that the tertiary, helical structure of the tropocollagen molecule begins to disappear and the elasticity of each covalent bond in the single strand governs the elastic response. This represents a significant distinction to the results obtained with reactive force fields, suggesting failure due to strain/force localization

small strains up to approximately 10% strain. The tensile stress for onset of permanent deformation (at around 43% strain) occurs at approximately 9.3 GPa, and the fracture stress is determined to be 11.2 GPa.

We have repeated the tensile deformation simulation for a single polypeptide out of the three making up the entire tropocollagen molecule. The strength of an individual polypeptide molecule is determined to be $0.713 \times 10^4$ pN, reached at about 37% tensile strain. This is significantly lower than that of the tropocollagen molecule (see Fig. 8.14, curve (c)).

### 8.3.3 Bending a Single Tropocollagen Molecule

We perform a computational experiment to describe the bending of a single tropocollagen molecule by clamping it at the boundaries and applying a force in the center of the molecule, as shown in Fig. 8.8(b). This is equivalent to the three-point bending test widely used in engineering mechanics. From the force–displacement data obtained by atomistic modeling, the bending stiffness $EI$ is given by

$$EI = \frac{dL^3}{48F_{\text{appl}}}, \tag{8.10}$$

where $F_{\text{appl}}$ is the applied force and $d$ is the bending displacement. Figure 8.15 depicts load versus displacement curves for various deformation speeds. Figure 8.16 depicts the resulting bending stiffness as a function of loading speed.

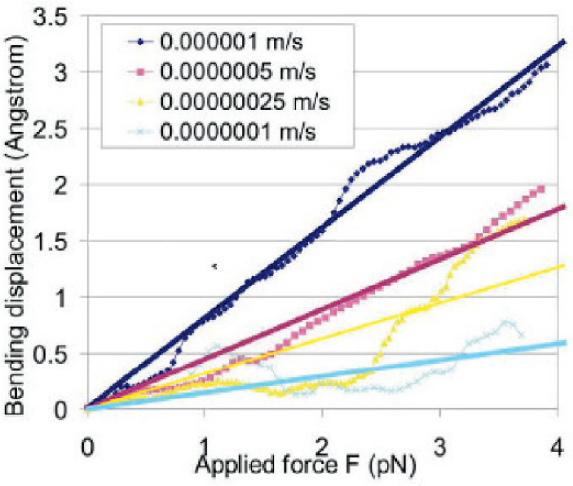


**Fig. 8.15** Bending displacement over bending force for the three-point bending test of a single tropocollagen molecule, as reported in Buehler and Wong (2007). Results are shown for various loading rates. The linear curves are linear fits to the MD simulation results

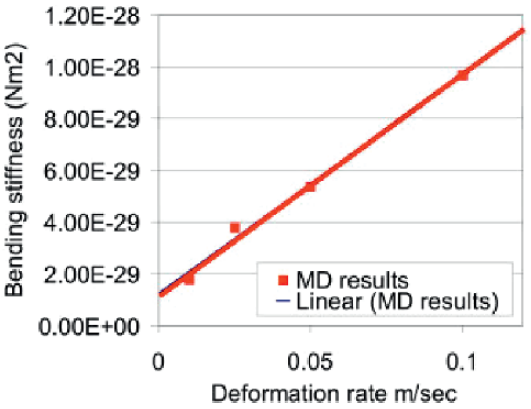


**Fig. 8.16** Dependence of bending stiffness EI of a single TC molecule on the deformation rate (based on results shown in Fig. 8.15) (Buehler and Wong 2007). The results indicate that EI decreases linearly with decreasing loading rate. A linear fit to the data enables us to extrapolate to smaller deformation speeds

### *8.3.4 Shearing Two Tropocollagen Molecules*

We continue with shearing experiments of an assembly of two tropocollagen molecules. The objective is to gain insight into the mechanisms and type of interactions between two tropocollagen molecules in aqueous solution. We start with a geometry as depicted schematically in Fig. 8.8(c). We first equilibrate the system without application of any mechanical shear load. We find that the equilibrium distance between two molecules depends on the presence of solvent; being reduced if solvent is present. With solvent present, we find an equilibrium distance between two tropocollagen molecules of $r_{EQ} \approx 16.52$ Å. All studies reported here are carried out with water molecules present. It is noted that this equilibrium distance leads to a molecular radius of 8.26 Å.

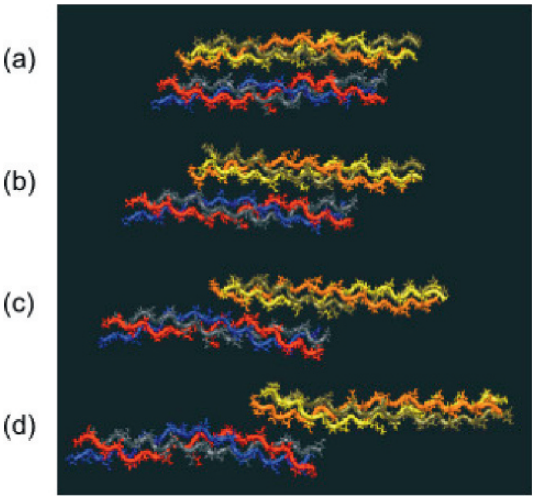


**Fig. 8.17** Snapshots of shearing of two tropocollagen molecules (Buehler 2006a). The subplots (**a**)–(**d**) show the behavior as the shear strain is increased

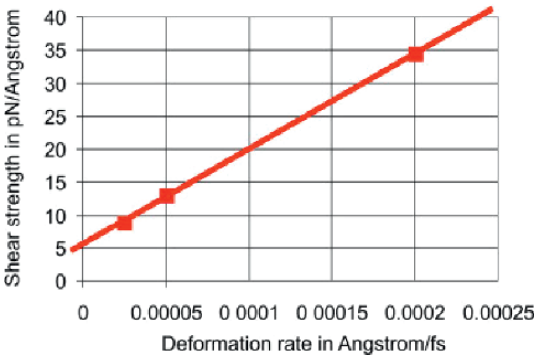


**Fig. 8.18** Atomistic modeling of shear experiments between two TC molecules (shear load applied using the SMD method) (Buehler 2006a). The plot shows the shear resistance as a function of loading rate, obtained by fully atomistic modeling using the CHARMM potential

Figure 8.17 depicts snapshots of the system as it undergoes shear deformation. Figure 8.18 depicts the maximum shear force versus pulling velocity as obtained during the shearing experiment.

We perform calculations with three different loading rates, $\dot{r}_\lambda = 0.0002$, 0.00005 and 0.000025 Å/step. We find that the resulting values are strain rate dependent. The maximum force decreases with decrease in loading rate, assuming values $F_{\max,\text{shear}} \approx 2,900\,\text{pN}$, $F_{\max,\text{shear}} \approx 1,100\,\text{pN}$ and $F_{\max,\text{shear}} \approx 750\,\text{pN}$, corresponding to the strain rates provided above. Using a linear extrapolation to vanishing loading rate, we estimate a maximum shear force of $F_{\max,\text{shear}} \approx 466\,\text{pN}$, corresponding to adhesion strength $\tau_{\max} = 5.55\,\text{pN/Å}$ (see Fig. 8.18). It is noted that the units of $\tau_{\text{shear}}$ are force/length (this is not a "stress" but rather adhesion force per unit length).

### *8.3.5 Development of a Mesoscopic, Molecular Model*

The atomistic modeling results, carried out at the level of individual polypeptide chains, tropocollagen molecules and assemblies of those, helped to develop a better qualitative and quantitative understanding of the competing mechanisms and forces during deformation of collagen, at a microscopic level. This information is now used to develop a mesoscopic model, in which beads connected by different types of springs represent collagen molecules, whereas all parameters are completely derived from atomistic calculations. The motivation for these studies is the desire to model larger length and time scales. This approach is similar to training empirical potentials from quantum mechanical data using the force-matching approach, as done successfully earlier for metallic systems (Ercolessi and Adams 1994). The geometrical approach of coarse graining is visualized in Fig. 8.19.

The reduction of degrees of freedom in the mesoscale model enables one to study very long tropocollagen molecules with lengths on the order of several hundred nanometers, as well as bundles of tropocollagen molecules. This approach enables reaching a "material scale" and makes the overall mechanics of the material accessible to atomic and molecular scale modeling.

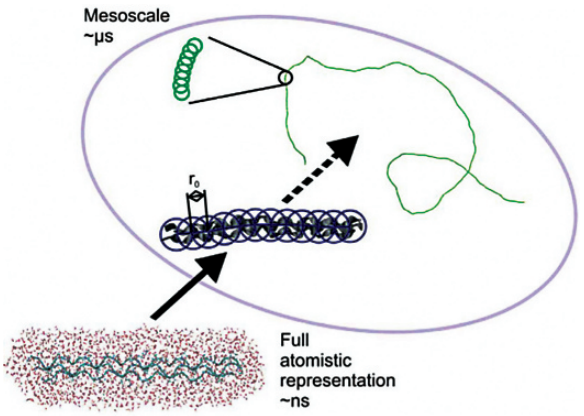


**Fig. 8.19** Schematic showing the development of the coarse-grained molecular model from a full atomistic description, illustrating the procedure utilized in various studies reviewed in this chapter. The full atomistic representation of the triple-helical TC structure is replaced by a collection of beads. The mesoscale model enables the treatment of ultra-long TC molecules at time and length scales not in reach by full atomistic models

#### 8.3.5.1 Model Development: Training from Pure Atomistic Results Using Energy and Force Matching

The goal is to develop the simplest model possible to perform large-scale studies of the mechanics of collagen molecules, eventually leading to understanding of the behavior of assemblies of such fibers. We assume that we can write the total energy of the system as

$$U = U_{\mathrm{T}} + U_{\mathrm{B}} + U_{\mathrm{weak}}. \tag{8.11}$$

The bending energy is given by

$$\phi_{\mathrm{B}}(\varphi) = \frac{1}{2} k_{\mathrm{B}} (\varphi - \varphi_0)^2 , \tag{8.12}$$

with $k_{\mathrm{B}}$ as the spring constant relating to the bending stiffness. The resistance to tensile load is characterized by

$$\phi_{\mathrm{T}}(r) = \frac{1}{2} k_{\mathrm{T}} (r - r_0)^2 , \tag{8.13}$$

where $k_{\mathrm{T}}$ refers to the resistance of the molecule to deform under tensile load. To account for the nonlinear stress–strain behavior of a single molecule under

tensile loading, we replace the harmonic approximation with a bilinear model (Buehler 2006a,b; Buehler and Wong 2007). The force between two particles is

$$F_{\mathrm{T}}(r) = -\frac{\partial \phi_{\mathrm{T}}(r)}{\partial r}, \tag{8.14}$$

where

$$\frac{\partial \phi_{\mathrm{T}}(r)}{\partial r}(r) = H(r_{\mathrm{break}} - r) \begin{cases} k_{\mathrm{T}}^{(0)}(r - r_0) & \text{if} r < r_1 \\ k_{\mathrm{T}}^{(1)}(r - \tilde{r}_1) & \text{if} r \geq r_1 \end{cases}. \tag{8.15}$$

In Eq. (8.15), $H(r - r_{\mathrm{break}})$ is the Heaviside function $H(a)$, which is defined to be zero for $a < 0$, and one for $a \geq 0$, and $k_{\mathrm{T}}^{(0)}$ as well as $k_{\mathrm{T}}^{(1)}$ for the small and large deformation spring constants. The parameter $\tilde{r}_1 = r_1 - k_{\mathrm{T}}^{(0)}/k_{\mathrm{T}}^{(1)}(r_1 - r_0)$ is determined from force continuity conditions. The function $U_{\mathrm{T}}$ is given by integrating $F_{\mathrm{T}}(r)$ over the radial distance.

In addition, we assume weak, dispersive interactions between either different parts of each molecule or different molecules, defined by a Lennard–Jones (LJ) function

$$\phi_{\mathrm{weak}}(r) = 4\varepsilon \left( \left[ \frac{\sigma}{r} \right]^{12} - \left[ \frac{\sigma}{r} \right]^{6} \right), \tag{8.16}$$

with $\sigma$ as the distance parameter and $\varepsilon$ describing the energy well depth at equilibrium.

Note that the total energy contribution of each part is given by the sum over all pair-wise and triple (angular) interactions in the system

$$U_{\mathrm{I}} = \sum_{\mathrm{pairs}} \phi_{\mathrm{I}}(r) \text{ and } U_{\mathrm{B}} = \sum_{\mathrm{angles}} \phi_{\mathrm{B}}(\varphi). \tag{8.17}$$

#### 8.3.5.2 Equilibrium Distances of Beads and Corresponding Masses

The mass of each bead is determined by assuming a homogeneous distribution of mass in the molecular model. The total mass of the tropocollagen molecule used in our studies is given by 8,152.2 amu. We divide the total length of the tropocollagen molecule used in the MD studies into $N_{\mathrm{MD}} = 6$ pieces, each bead containing five amino acid residues. Each bead then has a weight of 1,358.7 amu. Since the total length of the molecule is $L_0 = 84$ Å, the beads are separated by a distance $r_0 = 14$ Å (for a finer discretization of beads, say 7 Å, the mass will be half of this value). The beads represent different sequences in tropocollagen that when added together make the entire sequence.

#### 8.3.5.3 Dispersive and Non-bonding Interactions

The LJ parameters are determined from the calculations of shearing two collagen fibers. In all these considerations, we assume that a pair-wise interaction between different tropocollagen molecules is sufficient and that there are no multi-body contributions. Based on these assumptions, we model the interactions between different molecules using a LJ 12:6 potential. The distance parameter $\sigma$ is given by

$$\sigma = \frac{D}{\sqrt[6]{2}} \approx 14.72\,\text{Å}, \tag{8.18}$$

where $D$ is the equilibrium distance as measured in the MD simulations, $D = 16.52\,\text{Å}$.

The shear strength can be used to extract the LJ parameters for the weak, dispersive interactions between two fibers. Note that this interaction includes the effect of solvation water and other bondings (e.g., H-bonds, etc.).

The maximum force in a LJ potential, assuming a single LJ "bond" is given by

$$F_{\text{max,LJ}} = \frac{\Lambda\,\varepsilon}{\sigma}, \tag{8.19}$$

while noting that $\Lambda \approx 2.3964$ for the LJ 12:6 potential. The parameter $\sigma$ is already determined, leaving only $\varepsilon$ to be trained using a force-matching approach.

The parameter $\varepsilon$ can be obtained by requiring a force balance at the point of rupture:

$$F_{\text{max,LJ}} N_{\text{MD}} = \tau_{\text{max}} \quad L = F_{\text{max}}. \tag{8.20}$$

This expression can be used to determine $\varepsilon$ as

$$\varepsilon = \frac{F_{\text{max}}\,\sigma}{\Lambda\,N_{\text{MD}}}. \tag{8.21}$$

From atomistic modeling we calculate $F_{\text{max}}$ allowing to estimate numerical values for $\varepsilon$. We find that $\varepsilon \approx 11.06\,\text{kcal/mol}$ predicted from Eq. (8.21). Based on the extrapolation of shear force $F_{\text{max,shear}} \approx 466\,\text{pN}$ corresponding to vanishing strain rate we finally arrive at a value $\varepsilon \approx 6.87\,\text{kcal/mol}$.

Presence of intermolecular cross-links effectively leads to an increased intermolecular adhesion in the region where cross-links are formed, as discussed in Robins and Bailey (1973), Lodish et al. (1999) and Bailey (2001). To model the effect of cross-links, the adhesion parameter $\varepsilon_{\text{LJ}}$ is modified to account for the stronger interaction between molecules. Variation of the parameter $\varepsilon_{\text{LJ}}$ along the molecular axis enables one to account for specific spatial distributions of cross-links. Experimental analyses of the molecular geometry suggest that intermolecular aldol cross-links between lysine or hydroxylysine residues (Lodish et al. 1999; Alberts et al. 2002) primarily develop at the ends of tropocollagen molecules (Grandbois

et al. 1999; Lantz et al. 2001). The aldol cross-link is a C–C bond that forms between side chains of residues of two tropocollagen molecules.

The presence of cross-links is modeled by increased adhesion at the ends of each molecule, in segments of 60 Å to the left and right end of each tropocollagen molecule. According to this idea, the LJ potential parameter $\varepsilon_{\mathrm{LJ}}$ is increased by a factor $\beta \geq 1$ compared with the rest of the molecule in regions where cross-links are formed, and therefore

$$\varepsilon_{\mathrm{LJ,XL}} = \beta\, \varepsilon_{\mathrm{LJ}}. \tag{8.22}$$

For a choice $\beta = 12.5$, the additional shear force exerted at the end of the molecule corresponds to $\approx 4.2$ nN, which is on the order of the bond strength of covalent cross-link bonds (Buehler 2006). The parameter $\beta = 12.5$ therefore corresponds to the case when approximately one cross-link is present at each end of a tropocollagen molecule, leading to a cross-link density of $2.2 \times 10^{24}/\mathrm{m}^3$ (the cross-link density is defined as the number of cross-links per unit volume). Similarly, doubling the value $\beta = 25$ corresponds to two covalent cross-links.

#### 8.3.5.4 Tensile Spring Parameter

The tensile spring constant is determined from various calculations of stretch versus deformation, while being constrained to the regime of small loads and consequently small displacements. The spring constant $k_{\mathrm{T}}$ is then defined as

$$k_{\mathrm{T}} = \frac{N_{\mathrm{MD}} F_{\mathrm{appl}}}{\Delta d} = \frac{A_{\mathrm{C}}}{L_0} E, \tag{8.23}$$

with $\Delta d = L - L_0$ being the displacement of the atomistic model due to applied force $F_{\mathrm{appl}}$. Based on the low-strain rate tensile testing data discussed earlier, we find that $k_{\mathrm{T}}^{(0)} \approx 15.41\,\mathrm{kcal/mol/\AA^2}$. Similar considerations can be used to determine a value for $k_{\mathrm{T}}^{(1)}$, thereby considering the large deformation elastic behavior.

The parameters $r_1$ and $r_{\mathrm{break}}$ (unit: length) are related to the critical strains at which the tangent slopes in the stress–strain curve changes (denoted by $\varepsilon_1$, which is approximately 30%), and from the breaking strain (denoted by $\varepsilon_{\mathrm{break}}$, which is approximately 50%),

$$r_1 = (1 + \varepsilon_1) r_0. \tag{8.24}$$

$$r_{\mathrm{break}} = (1 + \varepsilon_{\mathrm{break}}) r_0. \tag{8.25}$$

#### 8.3.5.5 Bending Spring Parameter

Using an argument of energy conservation between the atomistic and the mesoscale model, we arrive at an expression for the bending stiffness parameter $k_{\mathrm{B}}$

$$k_B = \frac{3}{2}\frac{EI}{r_0}. \tag{8.26}$$

We find that $k_B \approx 14.98\,\text{kcal/mol/rad}^2$ as reported in Buehler and Wong (2007). These expressions are only valid for small deformations.

### 8.3.6 Validation of Mesoscale Model in Tensile Deformation

Figure 8.20 shows the force–displacement curve of a tensile stretching experiment of tropocollagen molecules, comparing results obtained with the CHARMM method, ReaxFF and the mesoscale model. The results confirm that the mesoscale model indeed approximates the results of reactive MD.

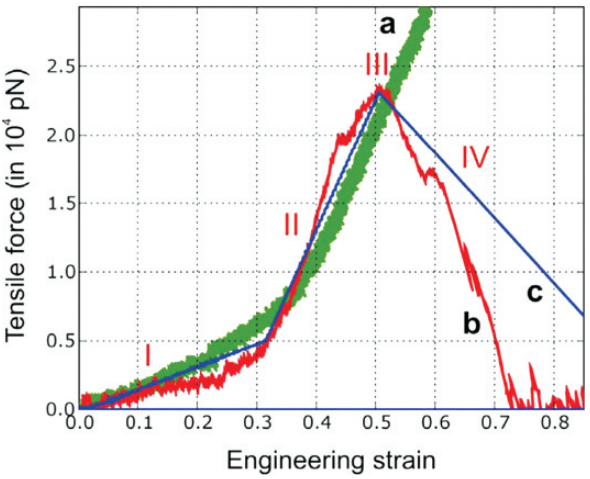


**Fig. 8.20** Modeling of a tensile stretching experiment of a TC molecule, comparing atomistic and mesoscale models for validation (using the SMD method) (results as reported in Buehler and Wong (2007)). The plot shows the force versus displacement of a TC molecule, using the CHARMM force field (curve "a") and the reactive ReaxFF force field (curves "b" and "c"). Curve "b" shows the force–displacement response of a single TC molecule, displaying three regimes. Regime I is characterized by uncoiling of the TC molecule, regime II is associated with a larger modulus due to stretching of covalent bonds and in regime III we observe fracture of the molecule, followed by a rapid decay of the force in regime IV. Curve "c" shows the results obtained using the reactive mesoscale model, illustrating the agreement between the different methods

### 8.3.7 Stretching an Ultra-long Tropocollagen Molecule: Mesoscale Modeling

The mesoscale model now enables direct comparison with experimental results, validating the major predictions of our model. The present section reviews molecular

simulation results reported in Buehler and Wong (2007) (for details regarding the modeling procedure see this reference).

Figure 8.21 shows a stretching experiment obtained by using the mesoscale model, as reported in Buehler and Wong (2007). Loading of the tropocollagen molecule starts from a coiled entangled configuration of the molecule with end-to-end distance of approximately 100 nm. During the initial regime (I), the molecule loses its entangled structure, while the applied forces remain relatively low. Once the contour length is reached ($x = L$), (II) uncurling of the triple helix, (III) stretching of covalent bonds in the individual polypeptides and (IV) rupture of the tropocollagen molecule occurs, followed by a sharp drop of the forces to zero. The qualitative behavior of tropocollagen molecules under stretch is similar to recent experimental studies carried out on collagen fibrils that reach forces on the order of μN, also showing a significant hyperelastic stiffening effect (Buehler and Wong 2007).

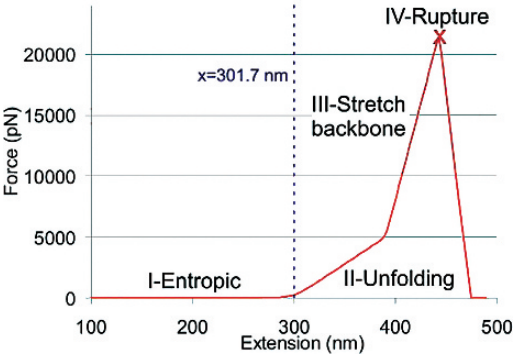


**Fig. 8.21** Force–displacement ($F(x)$) curves of stretching a single TC molecule, $L = 301.7$ nm, at 300 K, as reported in Buehler and Wong (2007). The plot depicts the force–displacement curve over the entire deformation range, covering four stages: (I) uncoiling of the entangled configuration, (II) uncurling of the triple helix, (III) stretching of covalent bonds in the individual polypeptides and (IV) rupture of the TC molecule. The dashed line indicates the contour length of the molecule

Figure 8.22 shows a zoom into the small-force regime, providing a quantitative comparison with optical tweezers experiments (Sun et al. 2002; An et al. 2004; Sun et al. 2004). The plot reveals very good agreement, even though the deformation rate in MD is still much higher.

### *8.3.8 Discussion and Conclusion*

We have reported atomistic modeling to calculate the elastic, plastic and fracture properties of tropocollagen molecules. Using full atomistic calculations, we presented a suite of calculations of different mechanical loading types to gain insight into the deformation behavior of tropocollagen molecules. Our results suggest that

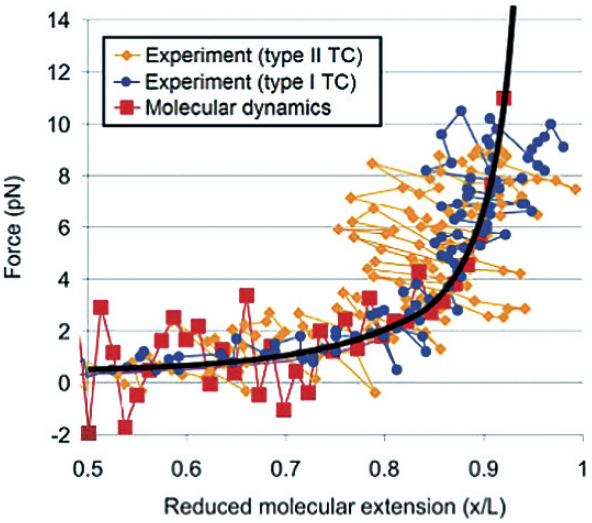


**Fig. 8.22** This plot depicts a subset of the results depicted in the previous figure, focusing on the small force, entropic response ($F < 14$ pN) (original results reported in Buehler and Wong (2007)). This plot also depicts experimental results obtained for TC molecules with similar contour lengths (Sun et al. 2002; An et al. 2004; Sun et al. 2004), as well as the prediction of the WLC model with persistence length approximately 16 nm

it is critical to include a correct description of the bond behavior and breaking processes at large bond stretch, information stemming from the quantum chemical details of bonding. A critical outcome of these studies is the observation that tropocollagen molecules undergo a transition from straight molecules to an S-shaped structure at increasingly large tensile stretch. As a consequence, we find that rupture of a single molecule does not occur homogeneously and thus at random locations, but instead, a local stress concentration develops leading to rupture of the molecule. Such information about the fracture behavior of collagen may be essential to understand the role of collagen components in biological materials. For example, the mechanics of collagen fibers at large stretch may play a critical role in the mechanical properties of bone during crack propagation, and elucidation of its mechanical response in particular at large strains is of critical importance during crack bridging in bone-like hard tissues (Ritchie et al. 2004).

We believe that reactive modeling that takes into account the complexity of chemical bonding may be critical to understand the fracture and deformation behavior of many other biological and protein-based materials. Further, we find a strong rate dependence of the mechanical properties, including Young's modulus. This is in agreement with the fact that collagen is known to be a viscoelastic material and suggests that this behavior may at least partly originate from processes and mechanisms at the molecular scale.

We find that the properties of collagen are scale dependent. For example, the fracture strength of individual polypeptides is different from the fracture strength of a tropocollagen molecule (see, e.g. Figure 8.14). The results further provide estimates of the fracture and deformation strength for different types of loading, enabling a comparison of different relative strengths.

The mesoscale model was used to predict the force-extension curve of a long tropocollagen molecule, including a direct and quantitative comparison with experimental results (as shown in Fig. 8.22).

## 8.4 Deformation and Fracture of Collagen Fibrils

Now we move up in the hierarchical scale to study the mechanics of assemblies of many tropocollagen molecules into a collagen fibril (see Fig. 8.3). Particular focus of this section is on studies of effects of the molecular length and cross-link densities. The present section reviews the molecular simulation results reported in Buehler (2006b) and Buehler (2008) (for details regarding the modeling procedure see these references).

### *8.4.1 Model Geometry and Molecular Simulation Approach*

A two-dimensional plane stress model of collagen fibrils with periodic boundary conditions in the in-plane direction orthogonal to the pulling orientation is considered here, with a periodic array of $2 \times 5$ tropocollagen molecules (total number of tropocollagen molecules is 10). The collagen fibrils show the characteristic staggered arrangement as observed in experiment. The plane stress condition is used to mimic the fact that the system is not periodic in the out-of-plane direction. Fully three-dimensional models are computationally very expensive. However, the model could treat such cases as well since there appears to be no intrinsic limitation of a two-dimensional case. No additional constraints other than the molecular interactions are applied to the system.

The simulations are carried out in two steps, (i) relaxation, followed by (ii) loading. Relaxation is achieved by slowly heating up the system, then annealing the structure at constant temperature, followed by energy minimization. Finite temperature calculations enable the structure to reassemble more easily, whereas energy minimization ensures finding the energetically optimal configuration of the molecules. If the initial relaxation is not carried out, pulling may be applied to a structure that is not in equilibrium and yield may be observed that is actually not due to the applied load but due to rearrangements toward the equilibrium structure. After relaxation, the structure displays the characteristics of collagen fibrils in agreement with experiment. To model tensile deformation of collagen fibrils, displacement boundary conditions are implemented by continuously displacing a set of particles in the boundary regions (in a region 40 Å to the left and right of the end of the collagen fibril).

The simulations are carried out by constantly minimizing the potential energy as the external strain is applied, where a displacement rate of 0.4 m/s is used for all simulations. Such rather high-strain rates are a consequence of the time scale

limitation of the molecular model; total time spans of several microseconds are the most that can be simulated since the time step has to be on the order of several femtoseconds.

As indicated above, the virial stress is used to calculate the stress tensor (Tsai 1979) for analyses of the stress–strain behavior. The yield stress $\sigma_Y$ is defined as the stress at which permanent deformation of the collagen fibril begins. This is characterized either by intermolecular shear or by molecular fracture, leading to permanent deformation. The yield strain $\varepsilon_Y$ is defined as the critical strain at which these mechanisms begin. The fracture stress $\sigma_F$ is defined as the largest stress in the stress–strain curve, corresponding to the maximum load the collagen fibril can sustain. The fracture strain $\varepsilon_F$ is the corresponding strain at which the largest stress occurs.

The strain is defined as $\varepsilon = (x - x_0)/x_0$, where $x_0$ is the initial, undeformed length of the collagen fibril, and $x$ is the current, deformed length. It is noted that the extension ratio or stretch $\lambda$ is related to the strain via $\lambda = 1 + \varepsilon$.

## *8.4.2 Size-Dependent Properties: Effects of Molecular Length*

Here we focus on atomistic and molecular modeling of the mechanical properties of collagen under large stretch, leading to permanent deformation or fracture. We show that the key to understanding the mechanics of collagen is to consider the interplay among the mechanics of individual tropocollagen molecules, the intermolecular chemical interactions and the mesoscopic properties arising from hundreds of molecules arranged in fibrils. We explore the mechanics of collagen by considering different nanostructural designs and pay specific attention to the details of molecular and intermolecular properties and its impact on the mechanical properties.

Under macroscopic tensile loading of collagen fibrils, the forces are distributed predominantly as tensile load carried by individual and as shear forces between different tropocollagen molecules (Buehler 2006a, b). Energetic effects rather than entropic contributions govern the elastic and fracture properties of collagen fibrils and fibers. The fracture strength of individual tropocollagen molecules is largely controlled by covalent polypeptide chemistry. The shear strength between two tropocollagen molecules is controlled by weak dispersive and hydrogen bond interactions and by some intermolecular covalent cross-links.

### 8.4.2.1 Theoretical Considerations: Homogeneous Shear

We first consider a simplistic model of a collagen fibril by focusing on a staggered assembly of two tropocollagen molecules (Buehler 2006b), as illustrated in Fig. 8.23. The shear resistance between two tropocollagen molecules, denoted as $\tau_{shear}$, leads to a contact length dependent force

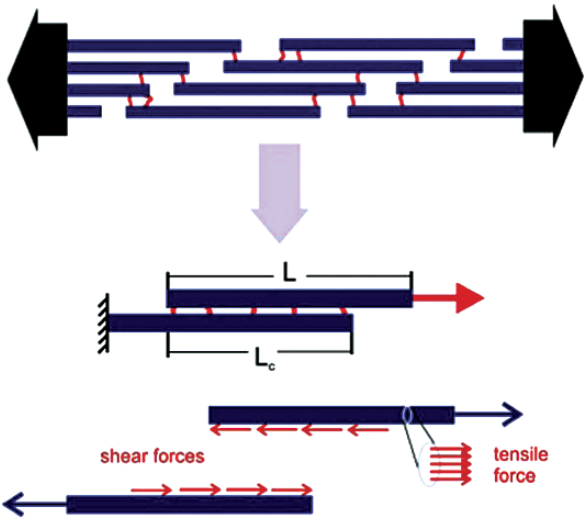


**Fig. 8.23** Simplistic representation of the staggered collagen fibril geometry as a simple bimolecular assembly. The lower part of the figure shows the distribution of intermolecular shear forces and tensile forces within each TC molecule

$$F_{\text{tens}} = \tau_{\text{shear}} L_C = \alpha \tau_{\text{shear}} L, \tag{8.27}$$

where $L_C$ is the contact length and $F_{\text{tens}}$ is the applied force in the axial molecular direction, which can alternatively be expressed as tensile stress $\sigma_{\text{tens}} = F_{\text{tens}}/A_C$ by considering the molecular cross-sectional area $A_C$. The parameter $\alpha$ describes the fraction of contact length relative to the molecular length, $\alpha = L_C/L$. Due to the staggered geometry, the shear resistance increases linearly with $L$, thus $F_{\text{tens}} \sim \tau_{\text{shear}} L$. This model holds only if shear deformation between the molecules is homogeneous along the axial direction.

### 8.4.2.2 Theoretical Considerations: Nucleation of Slip Pulses

An alternative to homogeneous intermolecular shear is propagation of slip pulses due to localized breaking of intermolecular "bonds". This analysis is based on a one-dimensional model of fracture initially proposed by Hellan (Griffith 1920; Hellan 1984). The model describes a one-dimensional strip of material attached on a substrate, which is under tensile loading in the axial direction. At a critical load, the energy released per advancement length of the adhesion front is equal to the energy required to break the bonding between the material strip and the substrate, leading to initiation of failure front. The failure front – corresponding to a dynamic crack tip – propagates at a fraction of the sound velocity, eventually displacing the material permanently in the direction of the applied load. We now apply this model to intermolecular deformation in collagen fibrils. The energy release rate is given by

$$G_0 = \frac{\sigma_R^2}{2E}, \tag{8.28}$$

where $E$ is Young's modulus of the tropocollagen molecule and $\sigma_R$ the applied stress. With $\gamma$ as the energy necessary to nucleate this defect, at the onset of nucleation the condition

$$G_0 = \gamma \tag{8.29}$$

needs to be satisfied (similar to the Griffith condition (Griffith 1920)). The detachment front corresponds to the front of decohesion. Bonds behind the fracture front reform, thus forming a "slip pulse". The slip pulse is a region with increased tensile strain in the tropocollagen molecule, which is several nanometers wide.

The existence of slip pulses is not a consequence of the discretization of the mesoscale model. Instead, this theoretical framework is developed based on continuum mechanics, assuming a homogeneous distribution of adhesive interactions along the molecular surface. In the spirit of Griffith's energy argument describing the onset of fracture, nucleation of slip pulses is controlled by the applied tensile stress $\sigma_R$, where

$$\sigma_R = \sqrt{2E\gamma}, \tag{8.30}$$

where $E$ is Young's modulus of an individual tropocollagen molecule and $\gamma$ relates to the energy required to nucleate a slip pulse.

When $\sigma_{tens} < \sigma_R$, deformation is controlled by homogeneous shear between tropocollagen molecules. However, when $\sigma_{tens} \geq \sigma_R$ intermolecular slip pulses are nucleated. This leads to a critical molecular length

$$\chi_S = \frac{\sqrt{2\gamma E}}{\tau_{shear}\alpha} A_C. \tag{8.31}$$

For fibrils in which $L < \chi_S$, the predominant deformation mode is homogeneous shear. When $L > \chi_S$, propagation of slip pulses dominates. The strength of the fibril is then independent of $L$ (Eq. (8.31)), approaching $\tau_{shear}\alpha\chi_S$. This concept is similar to the flaw tolerance length scale proposed for mineral platelets in bone (Gao et al. 2003).

The length scale $\chi_S$ depends on the material parameters and interaction between molecules. If $\gamma$ assumes very large values – for instance due to high cross-linking density, or due to the effects of solvents (e.g., low water concentration) – the tensile forces in each tropocollagen molecule (Eq. (8.27), or $F_{tens} \sim L$) reach the tensile strength of tropocollagen molecules, denoted by $F_{max}$, before homogeneous shear or slip pulses are nucleated ($F_{max}$ is a material constant that ultimately depends on the molecular structure of the tropocollagen molecule).

Considering $F_{tens} = F_{max}$ leads to a second critical molecular length scale,

$$\chi_R = \frac{F_{max}}{\tau_{shear}\alpha}. \tag{8.32}$$

This molecular length $\chi_R$ characterizes when the transition from molecular shear to brittle-like rupture of individual tropocollagen molecules occurs. The response of collagen fibrils to mechanical load changes from shear or glide between tropocollagen molecules, to molecular fracture as $L$ increases. For $L > \chi_R$, tropocollagen molecules break during deformation, whereas for $L \leq \chi_R$ deformation is characterized by homogeneous intermolecular shear.

The integrity of a complete collagen fibril is controlled by the strength of the weakest link. Thus, the interplay of the critical length scales $\chi_S/\chi_R$ controls the deformation mechanism.

When $\chi_S/\chi_R < 1$, slip pulse nucleation governs at large molecular lengths, whereas when $\chi_S/\chi_R > 1$, fracture of individual tropocollagen molecules occurs. For $L/L_\chi < 1$ homogeneous intermolecular slip dominates deformation. In both cases, the strength does not increase by making $L$ larger. The maximum strength of the fibril is reached at $L \approx L_\chi = \min(\chi_R, \chi_S)$. This is true for any arbitrary length $L$ of a tropocollagen molecule. Homogeneous shear deformation dominates below the critical molecular length $L_\chi$. For molecules with $L > L_\chi$, either slip pulses or fracture sets in, depending on which of the two length scales $\chi_S$ or $\chi_R$ is smaller. For short tropocollagen molecules, the strength of collagen fibrils tends to be small and depends on $L_C$. When $L \approx L_\chi$, the maximal tensile strength of fibrils is reached.

Further, choosing $L \approx L_\chi$ leads to maximized energy dissipation during deformation. The work necessary to separate two fibers in contact along a length $L_C$ under macroscopic tensile deformation is

$$E_{\text{diss}} = \int_{l=0}^{l=L_C} l\tau_{\text{shear}}\, \mathrm{d}l = \frac{1}{2} L_C^2 \tau_{\text{shear}}. \tag{8.33}$$

Equation (8.33) predicts an increase of the dissipated energy with increasing molecule length, therefore favoring long molecules. If $\chi_R < \chi_S$, the critical length $L_\chi$ constitutes an upper bound for $L_C$, since molecules rupture before shear deformation sets in. After bond rupture and formation of shorter molecules, $E_{\text{diss}}$ decreases significantly, suggesting that $L > L_\chi$ is not favored. Energy dissipation is at a maximum for $L \approx L_\chi$. If $\chi_S < \chi_R$, the dissipated energy can be approximated by (assuming $L_C > \chi_S$)

$$E_{\text{diss}} \approx \left( \frac{1}{2} \alpha^2 \chi_S^2 \tau_{\text{shear}} + (L_C - \alpha \chi_S) \cdot F_{\max} \right), \tag{8.34}$$

suggesting that after a quadratic increase for small molecular lengths, the dissipated energy increases linear with $L_C$.

### 8.4.2.3 Molecular Modeling of Mechanical Properties of Collagen Fibrils

We now model the deformation behavior of a more realistic fibril geometry as shown in Fig. 8.23 ("fibril", upper part), studying the change in mechanical properties due to variations in molecule length $L$.

Due to the staggered design of collagen fibrils with an axial displacement of about 25% of the molecular length, the contact length between tropocollagen molecules in a fibril is proportional to $L$. The length scales suggested in the previous section therefore have major implications on the deformation mechanics of collagen fibrils.

We consider fully hydrated cross-link-free collagen fibrils serving as a model for cross-link-deficient collagen. Figure 8.24 shows the stress versus strain response of a collagen fibril for different molecular lengths $L$. The results suggest that the onset of plastic deformation, the maximum strength and large-strain mechanics of collagen fibrils depends on the molecular length.

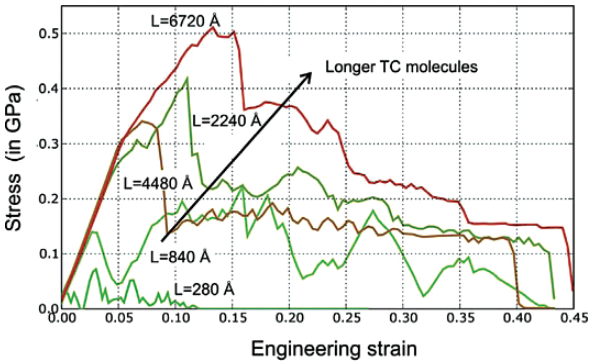


**Fig. 8.24** Stress versus strain of a collagen fibril, for different molecular lengths (model for cross-link-deficient collagen, as no covalent cross-links are present in the collagen fibril) (results as reported in (Buehler 2006)). The results suggest that the longer the molecular length, the stronger the fibril. The maximum elastic strength achieved by collagen fibrils approaches approximately 0.3 GPa, with largest stress around 0.5 GPa. The onset of intermolecular shear can be recognized by the deviation of the stress–strain behavior from a linear-elastic relationship

Figure 8.25 shows the normalized elastic strength of the fibril as a function of molecular length $L$. The results suggest an increase up to about 200 nm, then reaching a plateau value of around 0.3 GPa (results normalized by this value). The elastic uniaxial strains of collagen fibrils reach up to approximately 5%. The maximum stress reaches up to 0.5 GPa, during plastic deformation.

The molecular length at which the saturation occurs corresponds to a change in deformation mechanism, from homogeneous shear ($L \rightarrow 0$) to nucleation of slip pulses ($L \rightarrow \infty$). The corresponding molecular length provides an estimate for the critical molecular length scale $\chi_S \approx 200$ nm.

We note that $\chi_R \approx 436$ nm, as described in the previous section (it is a material property of the reference system). Therefore, the ratio $\chi_S/\chi_R < 1$, suggesting a

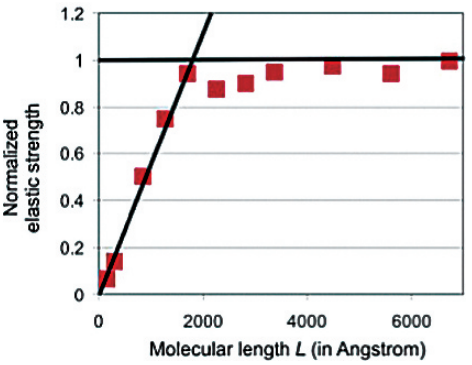


**Fig. 8.25** This plot shows the critical stress at the onset of plastic shear between TC molecules (Buehler 2006b). An initial regime of linear increase of strength with molecular length is followed by a regime of finite strength, at a plateau value

competition between slip pulses and homogeneous shear as the molecular length is varied. This suggests that cross-link-deficient collagen may predominantly undergo intermolecular shear deformation.

Figure 8.26 depicts the energy dissipated during deformation, per unit volume. We observe continuous increases with molecule length $L$, reaching a maximum at a critical molecular length $L_\chi$, then a slight decrease. Energy dissipation increases further at ultra large molecular lengths beyond 400 nm, due to longer shear paths during slip pulse propagation. The modest increase in energy dissipation for ultra-long molecules may be an inefficient solution, since assembling such ultra-long molecules into regular fibrils is challenging.

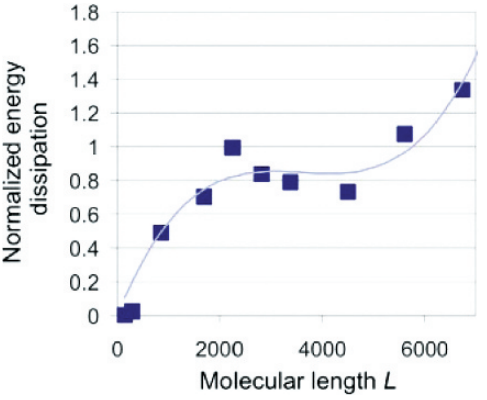


**Fig. 8.26** The plot depicts the dissipated energy during deformation, per unit volume, in a collagen fibril, as a function of molecular length, normalized by the maximum value (Buehler 2006b). An initial steep increase is followed by a plateau regime, with a local maximum around 220 nm. The smooth curve is a fit of a third-order expansion to the simulation data

#### 8.4.2.4 Discussion

The results suggest that the length of tropocollagen molecules plays a significant role in determining the deformation mechanics, possibly explaining some of the universal structural features of collagen found in Nature.

The two length scales $\chi_S$ and $\chi_R$ provide a quantitative description of the three different deformation mechanisms in collagen fibrils: (i) intermolecular shear, (ii) slip pulse propagation and (iii) fracture of individual tropocollagen molecules.

The governing deformation mechanism is controlled by the ratio $\chi_S / \chi_R$: Whether molecular fracture ($\chi_S / \chi_R > 1$) or slip pulses ($\chi_S / \chi_R < 1$) dominate deformation, the strength of the fibril approaches a maximum that cannot be overcome by increasing $L$. When $L_\chi = \min(\chi_R, \chi_S)$, tensile forces due to shear are in balance with either the fracture strength of tropocollagen molecules ($\chi_S / \chi_R > 1$) or with the critical load to nucleate slip pulses ($\chi_S / \chi_R < 1$). In either case, the maximum strength of the fibril is reached when $L \approx L_\chi$, including maximum energy dissipation.

When the length of collagen molecules is close to the critical length scale $L_\chi$, two objectives are satisfied: (i) Under large deformation, tropocollagen molecules reach their maximum strength without leading to brittle fracture and (ii) energy dissipation during deformation is maximized. This concept may explain the typical staggered geometry of collagen fibrils found in experiment, with extremely long molecules – leading to large energy dissipation during deformation.

The mechanisms of deformation and their dependence on the molecular design are summarized in a deformation map, shown in Fig. 8.27.

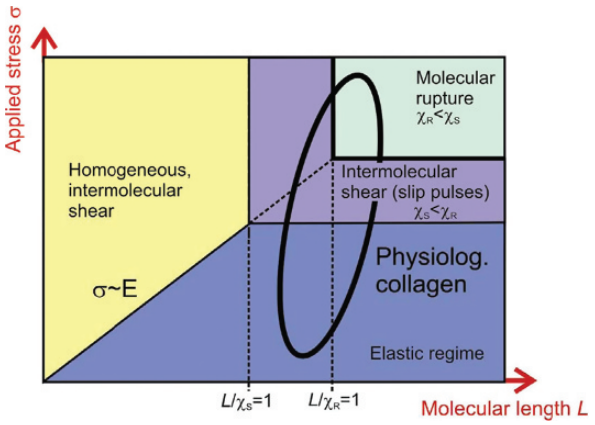


**Fig. 8.27** Deformation map of collagen fibrils, as reported in Buehler (2006b). The mechanical response is controlled by two length scales $\chi_S$ and $\chi_R$. Intermolecular shear governs deformation for small molecular lengths, leading to relatively small strength of the collagen fibril. For large molecular lengths, either intermolecular slip pulses ($\chi_S / \chi_R < 1$) or rupture of individual TC molecules ($\chi_S / \chi_R > 1$) dominate. This regime refers to the case of strong intermolecular interactions (e.g., increased cross-link densities). Physiological collagen typically features long molecules, with variations in molecular interaction, so that either intermolecular shear (e.g., slip pulses) or molecular fracture are predicted to dominate

Slip pulses are nucleated by localized larger shear stresses at the end of the tropocollagen molecules. Thus, cross-links at these locations provide a molecular-scale mechanism to prevent slip pulse nucleation, as this leads to an increase of the

energy required to nucleate slip pulses, thus to a larger value of $\gamma$. This results in an increase of $\chi_S$, due to the scaling law:

$$\chi_S \sim \sqrt{\gamma}. \tag{8.35}$$

As a consequence, the ratio $\chi_S/\chi_R$ increases, making collagen fibrils stronger. Remarkably, this nanoscale distribution of cross-links agrees with the natural collagen design seen in experiment, often showing cross-links at the ends of the tropocollagen molecules (Bailey 2001) (reminiscent of crack bridging (Nalla et al. 2003a,b; Ritchie et al. 2004)).

Cross-links provide additional strength to the fibrils, in agreement with experiment (Bailey 2001). However, extremely large cross-link densities lead to negative effects as the material is not capable to dissipate much energy during deformation – leading to a brittle collagen that is strong, but not tough. Such behavior is observed in dehydrated collagen, or in aged collagen featuring higher cross-link density (Bailey 2001). In contrast, decreased cross-linking as it occurs in the Ehlers–Danlos V disease (Lichtens Jr et al. 1973; Glorieux 2005) leads to significantly reduced tensile strength of collagen, as $\chi_S/\chi_R < 1$. The ratio $L/L_\chi$ decreases, resulting in skin and joint hyperextensibility due to extremely weak collagen tissue, incapable of dissipating significant energy.

Our model can be used to study different design scenarios. A design with many cross-links and short molecules would lead to a very brittle collagen, even in the hydrated state. Such behavior would be highly disadvantageous under physiological conditions. In contrast, long molecules provide robust material behavior with significant dissipation of energy (Fig. 8.26). Some experiments (Hulmes et al. 1995; Sasaki and Odajima 1996; Puxkandl et al. 2002; Sun et al. 2004; Bhattacharjee and Bansal 2005; Bozec et al. 2005) support the notion that cross-link-deficient collagen shows wide yield regions and large plastic deformation.

Both elastic strength and energy dissipation approach a finite value for large molecular lengths, making it inefficient to create collagen fibrils with tropocollagen molecules much longer than $L_\chi$, which is on the order of a few hundred nanometers (Fig. 8.25). This length scale agrees somewhat with experimental results of tropocollagen molecules with lengths around 300 nm.

Large deformation is a critical physiological condition for collagen-rich tissue. The risk of catastrophic brittle-like failure needs to be minimized in order to sustain optimal biological function. The nanoscale ultrastructure of collagen may be designed to provide robust material behavior under large deformation by choosing long tropocollagen molecules. Robustness is achieved by the design for maximum strength and maximized energy dissipation by shear-like mechanisms. The requirement for maximum energy dissipation plays a crucial role in determining the optimal molecular length $L_\chi$. The layered design of collagen fibrils plays a critical role in enabling long deformation paths with large dissipative stresses. This is reminiscent of the "sacrificial bond" concept (Hansma et al. 2007).

The properties of collagen are scale dependent (Sasaki and Odajima 1996). The fracture strength of an individual tropocollagen molecule (11.2 GPa) differs from

the fracture strength of a collagen fibril (0.5 GPa). Similarly, Young's modulus of an individual tropocollagen molecule is approximately 7 GPa, while Young's modulus of a collagen fibril is smaller, approaching 5 GPa (for $L \approx 224$ nm). This is in qualitative agreement with experiment.

Quantitative theories of the mechanics of collagen have many applications, ranging from the development of new biopolymers to studies in tissue engineering, where collagen is used as a scaffolding material. In addition to optimization for mechanical properties, other design objectives such as biological function, chemical properties or functional constraints may be responsible for the structure of collagen. However, the physiological significance of large mechanical deformation of collagen fibers suggests that mechanical properties could indeed be an important design objective.

### *8.4.3 Effect of Cross-Link Densities*

To understand the influence of cross-links on the deformation mechanics of collagen fibrils, a series of computational experiments of pulling individual collagen fibrils with increasing density of cross-links are carried out (Buehler 2008). All results are compared with a control system of a cross-link-free collagen fibril. Systematic increases of the density of cross-links enable one to observe the difference in mechanical behavior. Particular attention is paid to the small- and large deformation behavior and the effect of intermolecular cross-links on the mechanical properties and deformation mechanisms.

In particular, studies are carried out that focus on the changes in the elastic and fracture behavior of the collagen fibril as the parameters are varied. An analysis of the molecular mechanisms allows one to develop a mechanistic understanding of the deformation behavior of collagen fibrils.

Figure 8.28 visualizes how the molecular model describes the presence of intermolecular cross-links.

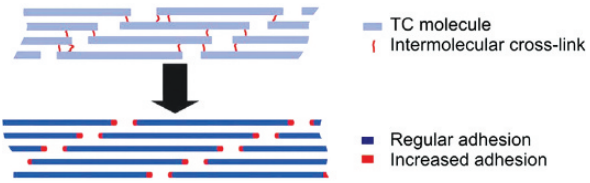


**Fig. 8.28** Schematic showing how the presence of cross-links is modeled by increased adhesion at the ends of each molecule, in segments of 60 Å to the left and right of each tropocollagen molecule. Implementing a variation of the amplification of the adhesion strength constitutes a simplistic model for varying cross-link densities. A parameter $\beta$ is introduced that describes the increase of adhesion at the ends of each TC molecule, so that $\tau = \beta \tau XL$ ($\tau$ is the adhesion force/length between two TC molecules). The parameter $\beta = 15$ corresponds to the case when approximately one cross-link is present at each end of a tropocollagen molecule

### 8.4.3.1 Tensile Deformation: Stress–Strain Curves

Figure 8.29 depicts the stress–strain curve for various cross-link densities, expressed in terms of the parameter $\beta$. For small values of cross-link densities ($\beta < 10$), the fibril starts to yield at strain in the range of 5–10% and shows rather long dissipative deformation paths, leading to fracture at strains between 50 and 100%.

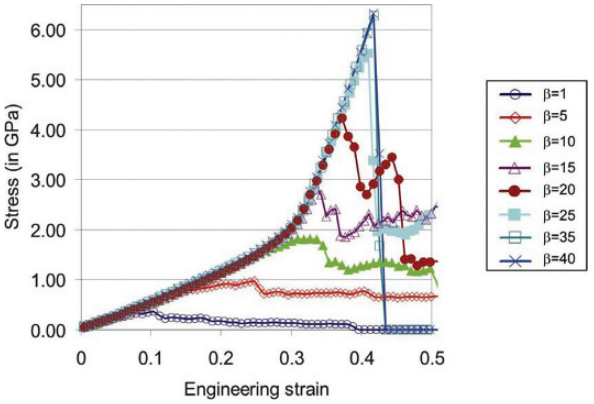


**Fig. 8.29** Stress versus strain of a collagen fibril, for different cross-link densities, as reported in Buehler (2008). The results clearly show that larger cross-link densities lead to larger yield strains, larger yield stresses as well as larger fracture stresses. For larger cross-link densities, the second elastic regime (seen as much steeper, second slope) is activated. As the cross-link density increases, the collagen fibril shows a more "brittle-like" deformation behavior. For values of $\beta >$ 25, the deformation mechanisms is characterized by molecular fracture, and as a consequence, the maximum fracture stress of the collagen fibril does not increase with increasing cross-link densities. This cross-link density corresponds to the case when two cross-links per molecule are present

It is found that larger cross-link densities lead to larger yield strains, larger yield stresses as well as larger fracture stresses. At a critical cross-link density corresponding to one cross-link per molecule ($\beta \approx 15$), the second, steeper elastic regime is activated. This strong increase in tangent modulus corresponds to stretching of the protein backbone. This molecular deformation mode dominates after the uncoiling of the tropocollagen molecule under breaking of H-bonds (Sasaki and Odajima 1996). The results clearly confirm the significance of the presence and density of cross-links on the deformation behavior.

Large elastic tensile strains of up to 50% are possible since each tropocollagen molecule itself can sustain strains of up to 50% tensile deformation (this is shown in Fig. 8.4, curve for a single tropocollagen molecule). In the collagen fibril, such large strains at the molecular scale are only possible if strong links exist which prevent molecular slip and therefore enable transfer of large loads to the individual tropocollagen molecules. As shown in this chapter, developing cross-links between molecules is a possible means of achieving this situation.

### 8.4.3.2 Comparison: Single Tropocollagen Molecule and Collagen Fibril

Figure 8.30 shows a comparison between the stress–strain curves of a collagen fibril ($\beta = 25$) and a single tropocollagen molecule, for tensile strains below 40%. Both structures are completely in the elastic regime (the tropocollagen molecule fractures at approximately 50% tensile strain and the collagen fibril starts to yield at slightly above 40% strain). These results show that the stresses in the single tropocollagen molecule are larger than in the collagen fibril.

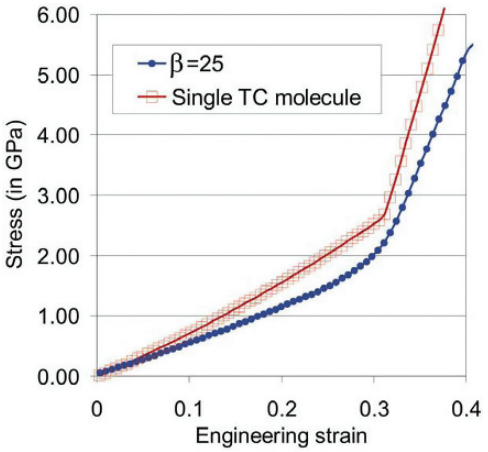


**Fig. 8.30** Stress versus strain, comparing a collagen fibril ($\beta = 25$) with a single TC molecule (Buehler 2008). Both structures are completely in the elastic regime (the TC molecule fractures at approximately 50% tensile strain and the collagen fibril starts to yield at slightly above 40% strain). This plot shows that the stresses in the single TC molecule are larger than in the collagen fibril and that the tangent modulus is larger throughout deformation. This agrees well with experimental results (Sasaki and Odajima 1996)

Figure 8.31 plots the tangent modulus of the stress–strain curve depicted in Fig. 8.30. The results clearly indicate that the tangent modulus of the single tropocollagen molecule is larger than that of a collagen fibril. The results suggest that the modulus of a single tropocollagen molecule is approximately 40% larger throughout deformation. This agrees well with experimental results, suggesting an increase of the stiffness from fibril to molecule close to 40% (Sasaki and Odajima 1996).

Even though cross-links are stiffer than the tropocollagen molecule itself, the overall density of cross-links is rather small so that the stiffening effect is negligible. The origin of the softening is the combination of rather weak intermolecular interactions with the single molecule elasticity along most of the axial length of the tropocollagen molecules. This leads to an effective softening of the fibrillar structure even when cross-links are present. This may change for extremely large cross-link densities, for example when cross-links form along the entire axial dimension of the chain.

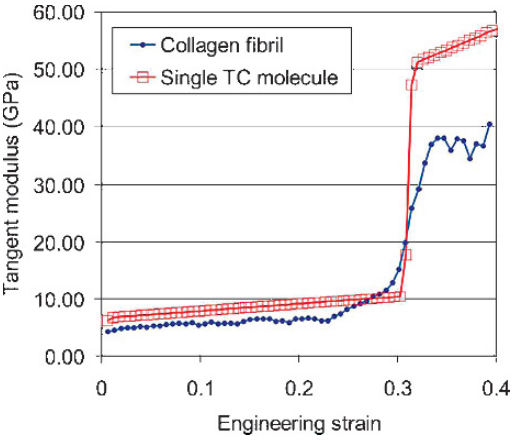


**Fig. 8.31** Tangent modulus versus strain, comparing a single TC molecule and a collagen fibril (cross-link parameter $\beta = 25$) (Buehler 2008). The results show that the tangent modulus of the single TC molecule is approximately 40% larger, except for the transition region during which the modulus of the fibril is larger (between 20 and 30% fibril strain)

### 8.4.3.3 Yield Stress and Fracture Stress Analysis

Figure 8.32 depicts the yield stress of a collagen fibril as a function of the cross-link density (curve "relative strength"). The plot shows that for larger cross-link densities, the material becomes stronger. However, when $\beta > 25$, the yield stress and fracture stress do not depend on the cross-link density any more as the yield stress reaches a plateau value. The plateau can be explained by a change in molecular deformation mechanism from predominantly intermolecular shear (for $\beta < 25$) to molecular fracture (for $\beta > 25$). Whereas the strength of the fibril is controlled by intermolecular adhesion for $\beta < 25$, the strength is dominated by the molecular fracture properties. This observation confirms a change in mechanisms as suggested in an earlier study (Buehler 2006b).

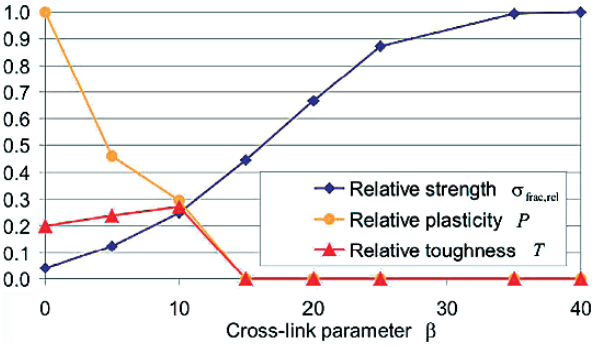


**Fig. 8.32** Relative strength $\sigma_{\text{frac,rel}}$, relative amount of plasticity $P$ as well as relative toughness of a collagen fibril $T$ as a function of the cross-link parameter $\beta$. For large cross-link densities $\beta > 15$, the material behavior becomes increasingly brittle and the failure strength (or yield strength, equivalently) saturates, as failure is controlled by rupture of individual TC molecules. The variation of the toughness $T$ suggests that a maximum relative toughness is reached for a cross-link parameter of approximately $\beta \approx 10$

As the cross-link density increases, the collagen fibril becomes more "brittle-like". The increasingly brittle character is clearly illustrated by the ratio of fracture stress versus yield stress. For smaller values of $\beta < 15$, the stress–strain curves show a stiffening effect after onset of yield, similar to work-hardening as known in metal plasticity. However, this stress increase decreases with increasing cross-link density. The data show that as the cross-link parameter exceeds 15, the material becomes "brittle-like", characterized by immediate drop of the stress after onset of yield without dissipative deformation.

An analysis of the stress–strain behavior provides further insight into the elastic and plastic deformation modes. The analysis of the stress–strain curves for varying cross-link densities corroborates the notion that for increasing cross-link densities, the material becomes increasingly "brittle-like".

Figure 8.32 further depicts the relative strength ($\sigma_{\text{frac,rel}} = \sigma_{\text{frac}}/\sigma_{\text{frac,max}}$), relative amount of plasticity (calculated with yield strain $\varepsilon_{\text{yield}}$ and yield stress $\varepsilon_{\text{frac}}$, $P = (\varepsilon_{\text{frac}}/\varepsilon_{\text{yield}} - 1)/(\max(\varepsilon_{\text{frac}}/\varepsilon_{\text{yield}}) - 1)$), as well as the relative toughness of a collagen fibril ($T = \sqrt{P \cdot \sigma_{\text{frac,rel}}}$) as a function of the cross-link parameter $\beta$. Hereby the "toughness" of a material is defined as the property of being both strong and requiring a lot of energy to break. The results suggest that an optimal relative toughness is reached for a cross-link parameter of $\beta \approx 10$. This value density corresponds to an approximate spacing of cross-links in the molecular axial direction of $\approx 420$ nm.

#### 8.4.3.4 Comparison with Experimental Results

This section is dedicated to a brief discussion of our computational results in light of recent experimental reports of stretching experiments of tropocollagen molecules and individual collagen fibrils.

Table 8.2 provides an overview of moduli obtained for single tropocollagen molecules. The comparison shows that our predictions for the moduli are close to experimental results, albeit they fall into the higher end of the range of values reported.

Table 8.3 summarizes results for elastic moduli of collagen fibrils from various sources. Unlike as for the single molecule case the agreement between experiment and simulation is not as good. A few important observations are discussed in more detail. Recently, MEMS devices were used to carry out tensile studies of single collagen fibrils (Eppell et al. 2006). The authors obtained a small-deformation modulus of approximately 0.4 GPa and a large deformation modulus of 12 GPa. The absolute values of the small-strain moduli are approximately 10 times smaller than in our simulation results.

One possible explanation for this disagreement could be entropic effects that may make the fibril softer in particular in the small-deformation regime. Such entropic effects are not considered in the present study, since all molecules are completely stretched out to their contour length at the beginning of the simulation and thus enter the energetic stretching regime instantaneously.

**Table 8.2** Comparison of Young's modulus of single tropocollagen molecules, experiment and computation

| Study/case and approach | Young's modulus |
|---|---|
| Single molecule stretching (Lorenzo and Caffarena 2005) – atomistic modeling | $4.8 \pm 1$ GPa |
| Single molecule stretching (Buehler 2006a) – reactive atomistic modeling | $\approx$ 7 GPa |
| Single molecule stretching (Vesentini, Fitie et al. 2005) – atomistic modeling | 2.4 GPa |
| X-ray diffraction (Sasaki and Odajima 1996) | $\approx$ 3 GPa |
| Brillouin light scattering (Harley, James et al. 1977) | 9 GPa |
| Brillouin light scattering (Cusack and Miller 1979) | 5.1 GPa |
| Estimate based on persistence length (Hofmann, Voss et al. 1984) | 3 GPa |
| Estimate based on persistence length (Sun, Luo et al. 2004) | 0.35–12 GPa |

**Table 8.3** Comparison of Young's modulus of collagen fibrils, experiment and computation

| Study, case and approach | Young's modulus |
|---|---|
| MEMS stretching of collagen fibrils (Ballarini et al. (Eppell, Smith et al. 2006)) | $\approx$ 0.4–0.5 GPa (small-strain modulus) $\approx$ 12 GPa (large-strain modulus) |
| X-ray diffraction (Gupta, Messmer et al. 2004) | 1 GPa |
| AFM testing (van der Rijt, van der Werf et al. 2006) | 2.7 GPa (ambient conditions) 0.2–0.8 GPa (aqueous media) |
| Molecular multi-scale modeling (Buehler 2006a,b; Buehler 2008) | 4.36 GPa (small-strain modulus) $\approx$ 38 GPa (large-strain modulus) |

Another possible reason may be the large deformation rates used in atomistic modeling, which often lead to overestimation of forces during mechanical deformation. Considering smaller deformation rates, for instance, may lead to smaller values for Young's modulus, as typically unfolding forces are larger for larger deformation rates (e.g., based on concepts related to Bell theory (Ackbarow et al. 2007; Buehler and Ackbarow 2007). Since the molecular model used in this study is based solely on atomistic input data, overestimation of the modulus value from the MD simulations will be transported throughout the multi-scale modeling scheme. This may explain why the values reported in the present work are close to the upper end of the range of experimental measurements.

However, the ratio of large-strain modulus to small-strain modulus is on the same order of magnitude, being between 24 and 30 in experiment and approximately 8.4 in simulation. The transition from small to large deformation modulus occurs at strains of approximately 30%, which is found in both experiment and simulation.

It has been suggested in Sasaki and Odajima (1996) and Borsato and Sasaki (1997) that the tensile strength may be greater than 1 GPa, which is corroborated by our results that suggest strengths ranging from 300 MPa (cross-link-deficient fibrils) to 6 GPa (highly cross-linked collagen fibrils). These values agree with the strengths predicted in our simulation (see Fig. 8.6, for example). On the

other hand, other results (Sasaki and Odajima 1996; Borsato and Sasaki 1997) show much lower failure stresses on the order of several MPa. Possible explanation for this discrepancy could be molecular defects, high loading rates or different geometries in those experiments that do not resemble the perfect patterns as considered in our study.

#### 8.4.3.5 Discussion

Molecular modeling has been employed to predict the small and large deformation mechanics of collagen fibrils, as a function of varying cross-link densities. The results suggest that the cross-link density governs the large deformation and in particular the yield or fracture mechanics. However, it influences the small-deformation mechanics only marginally (see, e.g., Fig. 8.29).

The model predicts that collagen fibrils are capable of undergoing extremely large deformation without fracturing; how much of this is elastic or dissipative depends on the cross-link densities. It is found that two prominent molecular mechanisms of permanent deformation dominate: molecular glide and molecular rupture.

Formation of covalent cross-links are essential to reach the elastically stiffer, second regime in the stress–strain curve of collagen, which corresponds to backbone stretching in the tropocollagen molecule. This phenomenon can be understood based on the mechanisms and the effect of the presence of cross-links: The increased traction at the end of the molecule allows for larger molecular strains to be reached. The larger strains give rise to larger overall yield and fracture stress. However, collagen fibrils become more "brittle-like" under these conditions as their ability to undergo dissipative, plastic deformation is reduced. These findings confirm some of the key hypotheses put forward in Bailey (2001), including effect of cross-links in making the material appear more "brittle", observed deformation mechanics and reduction of elastic modulus. This is confirmed by several analyses shown in Fig. 8.32, for instance.

The results improve the understanding of how molecular changes during aging contribute to modifications of tissue properties. Aging of organisms is primarily controlled by changes in the protein structure of elastin and collagen, when increased cross-linking between molecules develops due to non-enzymatic processes. These changes in the molecular architecture may lead to diseases that are induced by the modification of the mechanical properties of tissues. The analysis confirms that cross-linking indeed leads to stiffening and increasing "brittleness" of collagen-based tissues. It is noted that the results shown in Fig. 8.29 are in good qualitative agreement with the results of stress–strain responses of collagen during aging. Both the present model and experiment predict a stronger and less dissipative behavior with the development of additional cross-links.

It is found that the material properties of collagen are scale dependent. A softening of the modulus is observed when tropocollagen molecules are assembled into a collagen fibril. The modeling suggests a reduction of modulus on the order of 40%, which is close to experimental results (Sasaki and Odajima 1996) of similar comparisons between the mechanics of collagen fibrils and tropocollagen molecules

(see Fig. 8.30). This can also be found by taking a simple average value of all values for tropocollagen molecules reported in the literature (5.1 GPa, average of Table 8.2) divided by the average value of moduli for the collagen fibril (2.8 GPa, average of Table 8.3), which suggests an increase of modulus by approximately 80%.

The results show several features of the stress–strain behavior also found in experiment (Hulmes et al. 1995; Puxkandl et al. 2002; Eppell et al. 2006), notably the two regimes of moduli with a strong progressive stiffening with increasing strains. However, the magnitude of the stress is different, as MD modeling predicts larger stresses and larger moduli than seen in experiment.

A limitation of the present study is that spatial inhomogeneities of cross-link distributions are not considered. In principle, this can be implemented straightforwardly. Also, changes of molecular properties along the molecular length have not been considered, an important characteristic feature of many collagen-based tissues. This aspect is particularly significant to account for entropic effects that stem from more floppy labile regions of the tropocollagen molecules (Miles and Bailey 2001). These important aspects will be addressed in future work.

An improved understanding of the nanomechanics of collagen may help in the development of biomimetic materials, or for improved scaffolding materials for tissue engineering applications (Kim et al. 1999). Diseases such as Ehlers–Danlos (Lichtens Jr et al. 1973), osteogenesis imperfecta, scurvy or the Caffey disease (Glorieux 2005) are caused by defects in the molecular structure of collagen altering the intermolecular and molecular properties due to genetic mutations, modifying the mechanical behavior of collagen fibrils.

## 8.5 Nanomechanics of Mineralized Collagen Fibrils: Molecular Mechanics of Nascent Bone

One of the most intriguing protein materials found in Nature is bone, a material composed out of assemblies of tropocollagen molecules and tiny hydroxyapatite crystals, forming an extremely tough, yet lightweight material (Weiner and Wagner 1998; Currey 2002, 2005). Bone has evolved to provide structural support to organisms, and therefore, its mechanical properties are of great physiological relevance. Since collagen is the most fundamental building block of bone, here we review some insight into bone's smallest scale during bone formation (here referred to as nascent bone), mostly based on the study reported in Buehler (2007).

Mineralized collagen fibrils are highly conserved nanostructural building blocks of bone. By a combination of molecular dynamics simulation and theoretical analysis it is shown that the characteristic nanostructure of mineralized collagen fibrils is vital for its high strength and its ability to sustain large deformation, as relevant to the physiological role of bone, creating a strong and tough material. An analysis of the molecular mechanisms of protein and mineral phases under large deformation of mineralized collagen fibrils reveals a fibrillar toughening mechanism that leads to a manifold increase of energy dissipation compared to fibrils without mineral phase. This fibrillar toughening mechanism increases the resistance to fracture by forming

large local yield regions around crack-like defects, a mechanism that protects the integrity of the entire structure by allowing for localized failure.

As a consequence, mineralized collagen fibrils are able to tolerate micro-cracks on the order of several hundred micrometers size without causing any macroscopic failure of the tissue, which may be essential to enable bone remodeling. The analysis proves that adding nanoscopic small platelets to collagen fibrils increases their Young's modulus, yield strength as well as their fracture strength. It was found that mineralized collagen fibrils have a Young's modulus of 6.23 GPa (versus 4.59 GPa for the collagen fibril), yield at a tensile strain of 6.7% (versus 5% for the collagen fibril) and feature a fracture stress of 0.6 GPa (versus 0.3 GPa for the collagen fibril).

The work reviewed here (Buehler 2007; additional details regarding the numerical procedure can be found therein) is limited to the scale of mineralized fibrils, with the objective to provide insight into the most fundamental scales of bone and its deformation mechanics under tensile loading.

## *8.5.1 Introduction*

Figure 8.1 depicts the geometry of the nanostructure of bone, showing several hierarchical features from atomic to microscale. The smallest scale hierarchical features of bone include the protein phase composed of tropocollagen molecules, collagen fibrils (CFs) as well as mineralized collagen fibrils (MCFs) (see Fig. 8.33). Tropocollagen molecules assemble into collagen fibrils in a hydrated environment, which mineralize by formation of hydroxyapatite (HA) crystals in the gap regions

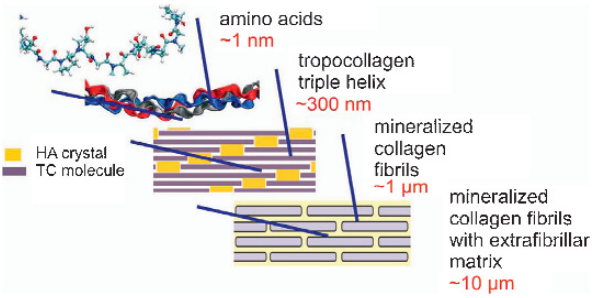


**Fig. 8.33** Geometry of the nanostructure of bone, showing several hierarchical features from atomic to microscale. Simple schematic of the hierarchical design of mineralized collagen fibrils, forming the most basic building block of bone (Weiner and Wagner 1998; Currey 2002). Three polypeptide strands arrange to form a triple-helical tropocollagen molecule. Tropocollagen molecules assemble into collagen fibrils in a hydrated environment, which mineralize by formation of hydroxyapatite (HA) crystals in the gap regions that exist due to the staggered geometry. Mineralized collagen fibrils combine with the extrafibrillar matrix to fibril arrays, which form fibril array patterns (Weiner and Wagner 1998; Currey 2002; Gupta et al. 2005). Typically, a total of seven hierarchical levels are found in bone. The present work is limited to the scale of mineralized fibrils, with the objective to provide insight into the most fundamental scales of bone and its deformation mechanics under tensile loading

that exist due to the staggered geometry. MCFs arrange together with an extrafibrillar matrix (EFM) to form the next hierarchical layer of bone. While the structures at scales larger than MCFs vary for different bone types, mineralized collagen fibrils are highly conserved, nanostructural primary building blocks of bone that are found universally (Thompson et al. 2001; Fratzl et al. 2004; Aizenberg et al. 2005; Fantner et al. 2005; Gupta et al. 2005; Gao 2006; Gupta et al. 2006; Tai et al. 2006). Each MCF consists of tropocollagen molecules with approximately 300 nm length, arranged in a characteristic staggered pattern. Gap regions in this arrangement are filled with tiny hydroxyapatite (HA) crystals. The present work is limited to the scale of mineralized fibrils, with the objective to provide insight into the most fundamental scale of bone and its deformation mechanics under tensile loading.

The mechanical properties of bone have received significant attention. Particular effort has been devoted to understanding the mechanisms that make bone tough. Whereas some experimental evidence suggests that the sub-micrometer structure is critical for the mechanical properties of macroscopic bone, other results indicate that macroscopic mechanisms such as crack bridging or micro-cracking contribute to the toughness of bone (Nalla et al. 2003a,b; Ritchie et al. 2004; Nalla et al. 2005; Ritchie et al. 2006). Concepts such as sacrificial bonds and hidden length (Thompson et al. 2001; Fantner et al. 2005; Hansma et al. 2007) suggest toughening mechanisms that occur between different mineralized collagen fibrils.

However, due to the structural complexity of bone, the analysis and quantification of the deformation mechanisms at the ultra-scale of individual mineralized collagen fibrils (MCFs) remains an area that is not well understood. Limited knowledge exists whether, and if yes, how molecular scale mechanisms within single MCFs contribute to the toughness and stiffness of bone, as well as for its ability to repair itself. The effect of precipitating mineral crystals during bone formation remains unknown.

Most theoretical and computational analyses of bone have been carried out at continuum scales, neglecting the particular complexities of molecular interactions and chemistry. To date, there exists no molecular model of the nanostructure of bone that enables a rigorous linking between molecular and tissue scales. It is emphasized that previous atomistic and molecular models of collagen fibrils (described in the previous sections) have not included any mineral phase (Buehler 2006b).

In the studies reported here, a simple molecular model of MCFs is utilized that provides a fundamental description of its nanomechanical properties. The small and large deformation mechanics of a pure collagen fibril and a mineralized collagen fibril are systematically compared (see Fig. 8.34 for a comparison of the two model systems). Both structures are subject to identical tensile loading in the direction of the molecular axis of the tropocollagen molecules. Comparing the deformation mechanisms, stress–strain behavior and energy dissipation reveals insight into the effect of mineralization. It is found that mineralization leads to an increase in stiffness, yield stress, fracture stress and energy dissipation. The study reveals how a highly dissipative, yet strong material can be formed out of a soft polymeric collagen phase and hard, brittle HA by arranging molecules and crystals at characteristic nanostructured length scales.


**Fig. 8.34** Overview of the two structures considered here; subplot (a) shows a CF and subplot (b) shows a MCF (original study reported in Buehler 2007). The structures are loading in uniaxial tension along the axis of the TC molecules

## *8.5.2 Molecular Model*

The computational model is developed with the aim to elucidate generic behavior and deformation mechanisms of MCFs.

The model is a simple 2D system of a mineralized collagen fibril, based on the model of pure collagen fibrils discussed above, here extended to describe an additional mineral phase. The CF consists of a staggered array of tropocollagen molecules. The gap zones in the CF are filled with a single crystal that has a planar size of approximately $28 \times 1.4$ nm, filling the entire open space, resembling the presence of the HA phase, leading to a MCF.

It is noted that as bone is formed, mineral crystals exceed the size of the gap region and penetrate into the collagen phase. The present study does not include these effects and is thus limited to the early stages of bone formation ("nascent bone"). The term "hydroxyapatite" (HA) is used to refer to the mineral phase in bone, although this component is also referred to as "dahllite" or carbonated apatite.

The study reviewed in this section is the first molecular-scale model of the nanostructure of bone. The experimental paper (Gupta et al. 2004) considers a geometry that is closest to the one considered in this chapter. However, to the best of our knowledge no other molecular scale model of the nanostructure of bone has been reported thus far.

The studies are carried out using a reactive mesoscopic model describing tropocollagen molecules as a collection of beads interacting according to interparticle multi-body potentials; the pure collagen model described in Buehler (2006b) is extended here to describe the HA phase and HA–TC interactions. The equations of motion are solved according to a classical molecular dynamics (MD) scheme implemented in the LAMMPS simulation code (Plimpton 1995).

The total potential energy of the model is

$$U = U_{\mathrm{T}} + U_{\mathrm{B}} + U_{\mathrm{TC}} + U_{\mathrm{HA}} + U_{\mathrm{HA-TC}}. \tag{8.36}$$

The difference to the model for pure collagen fibrils is extended here by two terms, $U_{\mathrm{HA}}$ (potential function for HA phase) and $U_{\mathrm{HA-TC}}$ (interaction potential HA–TC). The terms $U_{\mathrm{T}}$ and $U_{\mathrm{B}}$ are only applied within the tropocollagen molecules, as described above.

Intermolecular interactions between tropocollagen particles, HA particles and between HA and tropocollagen particles are described by a Lennard–Jones 12:6 (LJ) potential

$$\phi_{\mathrm{TC/HA/HA-TC}}(r) = 4\varepsilon\left(\left[\frac{\sigma}{r}\right]^{12} - \left[\frac{\sigma}{r}\right]^{6}\right), \tag{8.37}$$

with $\sigma$ as the distance and $\varepsilon$ as energy parameter, defined separately for different materials.

Model parameters for tropocollagen properties and interactions are identical as in the pure collagen model. The parameter $\varepsilon_{\mathrm{MF}} = 26.72\,\mathrm{kcal/mol}$, with $\sigma_{\mathrm{MF}} = 3.118\,\text{Å}$, which leads to a Young's modulus of $E_{\mathrm{HA}} \approx 135\,\mathrm{GPa}$. These parameters are determined by fitting against the experimentally determined elastic modulus of HA. This 2D LJ model leads to extremely brittle material behavior (Buehler et al. 2004), thus providing a good model for the physical and mechanical properties of the HA phase.

Interactions between the HA crystal and tropocollagen molecules are described by a LJ potential with $\sigma_{\mathrm{MF-TC}} = 7\,\text{Å}$. The adhesion strength in this potential is chosen to be $\varepsilon_{\mathrm{MF-TC}} = 25\,\mathrm{kcal/mol}$ for all HA–TC interactions, while the beginning and end of each tropocollagen molecule interacts with $\varepsilon_{\mathrm{MF-TC}} = 15\,\mathrm{kcal/mol}$. The distinction of interaction mimics weaker adhesion between HA and tropocollagen at the head of each tropocollagen molecule due to smaller contact area. The choice of these parameters corresponds to interface surface energies of $\gamma_{\mathrm{MF-TC}} \approx 0.375\,\mathrm{J/m^2}$ and $\gamma_{\mathrm{MF-TC}} \approx 0.225\,\mathrm{J/m^2}$.

Classical MD is used to solve the equations of motion by performing a continuous energy minimization of the system as the loading is increased, with a time step of 55 fs. After energy minimization and relaxation of the initial structure, loading is applied by displacing a thin layer of particles at the ends of the system with a strain rate $7.558 \times 10^{-8}$ per integration step. Periodic boundary conditions are applied in the direction orthogonal to pulling mimicking an infinitely large fibril, subject to uniaxial tensile loading.

It is emphasized that this simple model of the molecular and physical behavior of the nanocomposite is designed to deliberately avoid modeling the atomistic details of bonding within the HA crystal or across the HA–TC interface. However, it enables one to model the inhomogeneous stress and strain fields as well as the fracture behavior. Thus, the model system enables some first fundamental insight into the nanomechanics of mineralized fibrils.

### *8.5.3 Computational Results: Elastic, Plastic Regime and Fracture*

Figure 8.35 plots the stress–strain response of a pure collagen fibril (CF) compared with that of a MCF, under tensile loading, for tensile strains up to 50%. The stress–strain response for CF and MCF is qualitatively and quantitatively different, indicating that precipitation of HA crystals during bone formation significantly alters

the material response. The MCF features a larger strength and much increased energy dissipation under deformation. Plastic deformation starts at approximately 6.7% tensile strain for the mineralized fibril, whereas it occurs at approximately 5% tissue strain in the case of a pure CF. Further, the MCF shows significant softening at larger strains, with a characteristic sawtooth-shaped stress–strain curve due to repeated intermolecular slip. The mineralized fibril features a higher stiffness than the pure collagen fibril.

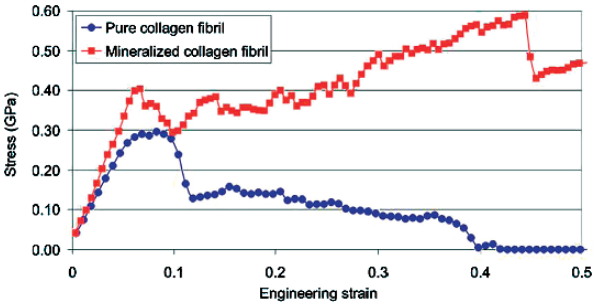


**Fig. 8.35** Stress–strain response of a mineralized collagen fibril (MCF) and a nonmineralized, pure collagen fibril (CF) (Buehler 2007). The plot shows the stress–strain curve, for the entire deformation up to tensile tissue strains of 50%. It is apparent that the MCF features a larger strength and much increased energy dissipation under deformation. Plastic deformation starts at approximately 6.7% tensile strain for the mineralized fibril, whereas it occurs at approximately 5% tissue strain in the case of a pure CF. The MCF shows significant softening at larger strains, with a characteristic sawtooth-shaped stress–strain curve due to repeated intermolecular slip. The mineralized fibril is stiffer than the pure collagen fibril

Figure 8.36 shows snapshots of the molecular geometry under increasing tensile load, clearly showing the deformation mechanism of intermolecular slip. Figure 8.36(a) shows snapshots of the deformation mechanisms of pure CF. Fibrillar yield is characterized by intermolecular slip (see red circle highlighting a local area of repeated molecular slip). Slip leads to formation of regions with lower material density. Figure 8.36(b) displays snapshots of the deformation mechanisms of MCFs. Slip initiates at the interface between HA particles and tropocollagen molecules. Slip reduces the density, leading to formation of nanoscale voids.

The details of the differences between the MCF and CF and associated deformation mechanisms will be discussed in the following sections.

#### 8.5.3.1 Elastic and Plastic Deformation

Up to the onset of yield, the mechanical response of the MCF is elastic (within the range of normal physiological function). In this regime, the increase of tissue strain leads to continuous increase of the strain in each tropocollagen molecule. Both MCF and CF display a linear-elastic regime for small deformation. The MCF is 36% stiffer than the CF (Young's modulus of a CF is 4.59 GPa versus 6.23 GPa for a MCF). The presence of HA crystals further changes the onset of plastic deformation,

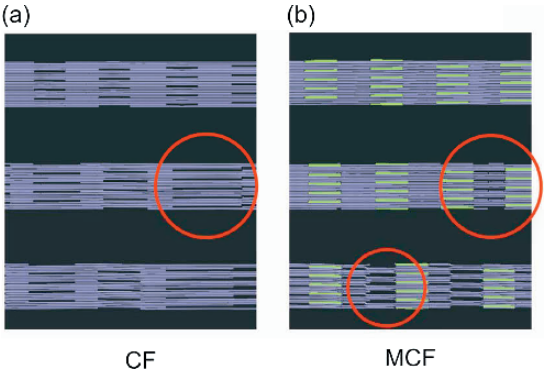


**Fig. 8.36** Molecular geometry of plastic deformation (Buehler 2007). Subplot (**a**): Snapshots of the deformation mechanisms, pure CF, for increasing strain. Fibrillar yield is characterized by intermolecular slip (see circle highlighting a local area of repeated molecular slip). Slip leads to formation of regions with lower material density. Subplot (**b**): Snapshots of the deformation mechanisms, MCF, for increasing strain. Slip initiates at the interface between HA particles and TC molecules. Slip reduces the density, leading to formation of nanoscale voids

characterized by a sudden drop in the stress–strain response. Whereas the CF begins to yield at approximately 5%, the MCF yields at 6.7%. This represents a 34% increase in yield strain. These results are summarized in Table 8.4. The data shown in Table 8.4 was generated based on the stress–strain curve shown in Fig. 8.35.

After onset of yield, the stress does not drop to zero rather quickly, but instead remains at levels of 0.4 GPa, with a slight increase with strain, approaching 0.6 GPa. After onset of yield, the MCF becomes softer, that is, less force is required for identical extension. The reduction in slope is due to the fact the strain in some of the tropocollagen molecules does not increase with tissue strain, since an increasing

**Table 8.4** Quantitative comparison of the deformation and fracture properties of CFs and MCFs (tensile strains up to 50%), as reported in (Buehler 2007)

| Property | CF | MCF | Ratio value MCF/CF |
|---|---|---|---|
| Young's modulus (small deformation) | 4.59 GPa | 6.23 GPa | 1.36 |
| Yield strain | 5% | 6.7% | 1.34 |
| Maximum stress | 0.3 GPa | 0.6 GPa | 2 |
| Failure mode | Molecular slip | Molecular slip and slip along HA–TC interface | N/A |
| Energy dissipation | 3.83 $GJ/m^3$ | 19.48 $GJ/m^3$ | $\approx 5$ |
| Ratio of TC strain versus tissue strain | Approaches 87% at yield | Approaches 100% at yield | 1.15 |
| Ratio of HA strain versus tissue strain | N/A | 11% | N/A |
| Size of fracture process zone $\xi_{cr}$ | $\approx 150\mu m$ | $\approx 200\mu m$ | 1.33 |

number of bonds to HA crystals and other tropocollagen molecules are broken. When fracture occurs, all molecular bonds inside the MCF are broken and the strains inside each component drops to zero.

Both CF and MCF yield by intermolecular slip. Repeated glide between tropocollagen molecules and between HA particles and tropocollagen molecules initiating by slip at the HA–TC interface enables a large regime of dissipative deformation after beginning of yield. In the case of the MCF, larger stresses can be maintained after initiation of slip due to additional resistance to slip at the interface between the tropocollagen molecules and HA particles. Mineralization of the CF leads to increase in strength by a factor of two. Most importantly, mineralization leads to a fivefold increase in energy dissipation.

#### 8.5.3.2 Molecular Mechanisms of Deformation and Toughening

An analysis of the strain field within tropocollagen molecules and HA platelets reveals that the observations discussed in the previous section can be explained by molecular nanomechanical mechanisms, since mineralization significantly changes the strain distribution.

In pure CF, the tissue strain (applied strain) is always larger than the strain within tropocollagen molecules, reaching approximately 87% immediately before yield begins.

In MCF, the tissue strain and tropocollagen strain remain much closer during deformation, approaching similar strain levels at the onset of plastic deformation. This is due to the good adhesion between HA platelets and tropocollagen molecules, which hinders initiation of intermolecular slip. The HA phase carries up to 11% of the tissue strain. Such large tensile strains correspond to a stress of several GPa. Evidence for the molecular failure mechanisms of intermolecular slip is also found in experiment, as for instance shown in Gupta et al. (2004).

#### 8.5.3.3 Comparison with Experimental Results

The most direct comparison of our molecular simulation results can be done with a recent experimental study reported in Gupta et al. (2004). We briefly summarize the main findings. By carrying out tensile tests of MCFs obtained from mineralized turkey leg tendon, it was shown that the stiffness increases continuously with increasing mineral content. It was shown that different mineralization stages correspond to stiffness values from 500 MPa (low mineral content) to 3 GPa (high mineral content). Further, the experiments revealed that the stress–strain behavior shows a characteristic softening behavior: An initial, rather stiff regime persists up to strains of approximately 3%, which is followed by a significant softening. The observed stress–strain response is reminiscent of a bilinear softening stress–strain behavior.

The mechanical behavior calculated based on the molecular model of MCF reported in this chapter agrees with several observations made in experiment (Gupta et al. 2004). For example, the MCF yield strain is somewhat close to experimental results (3% in experiment and 6.7% in simulation) (Gupta et al. 2004).

Further, the reduced slope at large strains agrees qualitatively with experiment (Gupta et al. 2004).

The finding that Young's modulus increases is in qualitative accordance with experiment (Gupta et al. 2004) comparing mineralized and non-mineralized tendon CFs. Experimental results suggest a continuous increase in Young's modulus under mineralization, ranging up to a factor of 3 for high mineral content (Borsato and Sasaki 1997; Gupta et al. 2006).

Further, the finding that component strains are smaller than tissue strains are consistent with experiment in bone (Screen et al. 2004) and tendon (Taylor et al. 2007), albeit these studies were carried out at larger scales. The results prove that this is also true at the smallest hierarchical scale of bone.

#### 8.5.3.4 Local Yield Protects the Integrity of the Entire Structure

The fracture process zone describes the geometric extension of the region around a crack-like flaw that undergoes plastic deformation when the specimen is loaded. For brittle materials, the fracture process zone is extremely small, limited to a few atomic distances. In ductile materials, the fracture process zone can become very large, approaching the specimen dimensions.

The size of the plastic, dissipative zone for a crack oriented orthogonal to the alignment direction of tropocollagen molecules can be approximated as

$$\xi_{\mathrm{cr}} \approx \frac{2\gamma E}{\sigma_{\mathrm{max}}^2}, \tag{8.38}$$

where $\sigma_{\mathrm{max}}$ is the maximum fracture stress, $\gamma$ is the energy necessary to create a new surface and $E$ is Young's modulus. Equation (8.38) shows that the size of the fracture process zone is proportional to the fracture surface energy. Thus increases in the dissipative work required to create two new surfaces lead to much larger plastic zones.

Based on the parameters extracted from molecular simulation (numerical values for $E$ and $\sigma_{\mathrm{max}}$ are given in Table 8.4; $\gamma = 11,460\,\mathrm{J/m^2}$) $\xi_{\mathrm{cr}} \approx 400\,\mu\mathrm{m}$ for MCFs.

This length scale has another important implication: For any defect smaller than $\xi_{\mathrm{cr}}$, fracture will not be controlled by the presence of this flaw. The material is insensitive to the presence of crack-like flaws below this characteristic defect dimension.

Notably, this length scale is on the same order of magnitude as small microcracks typically found in bone, with characteristic dimensions of several hundred micrometer diameter (Turner 2006; Taylor et al. 2007). It may also play a significant role in bone remodeling. Bone is remodeled in so-called basic multi-cellular units – BMUs – a combination of osteoclasts and osteoblasts forming small cavities inside the tissue. It has been shown that BMUs represent defects with dimensions of approximately 200 μm, thus on similar orders of magnitude as $\xi_{\mathrm{cr}}$ (Buehler et al. 2006). Thus the particular properties of MCF could be a vital component in allowing the presence of BMUs inside the tissue without compromising its strength.

Further, by limiting the dimensions of individual MCF in the hierarchical structure, failure will occur homogeneously within each MCF, with plastic strains distributed over the entire geometry.

This analysis provides insight into how the particular MCF structure contributes to toughness by comparing a pure HA crystal. The surface energy of pure HA ranges from 0.3 to 1.6 $J/m^2$ (density functional theory calculations (Zhu and Wu 2004), leading to a rather small fracture process zone on the order several nanometers. Thus any larger crack-like defect will lead to catastrophic failure. The estimate for $\gamma$ of a MCF obtained from MD studies of a fibril is several orders of magnitudes higher. Even though the modulus is much reduced in comparing a pure HA crystal with the MCF, the significant increase in $\gamma$ outruns the reduction in modulus. Further, the fact that $\sigma_{max}$ is smaller further leads to increase in the length scale.

In comparison with a CF, the MCF has a larger fracture process zone due to an increase in $\gamma$ as well as an increase in $E$. The effect of these two parameters outruns the effect of a smaller $\sigma_{max}$.

## *8.5.4 Discussion*

The work overcomes the limitations of the existing models of bone by explicitly considering tropocollagen molecules interacting with HA phases, providing a physics-based material description that enables one to make direct links between molecular structure, topology and fracture behavior. It is found that the nanostructural arrangement of the MCF is key to its mechanical properties, notably by allowing molecular slip as a major toughening mechanism.

In the following sections, implications of the findings for the understanding of bone formation and bone mechanics are discussed.

### 8.5.4.1 Hierarchical Toughening Mechanisms

Past research has revealed that toughening occurs at different scales. Our studies and results from investigations at other length scales suggest that each level in the hierarchy of bone may be designed to provide optimal toughness, thus being capable of taking advantage of nanoscale molecular and crystal properties, at larger scales.

The behavior discussed in this chapter is qualitatively similar to that suggested by the sacrificial bond model (Thompson et al. 2001). However, the mechanism described here operates at a smaller length scale in bone's structural hierarchy and has a different nanostructural origin; it is closely linked to the particular staggered molecular structure of the collagen fibrils and does not involve presence of metal ions. It is found that at the level of individual MCF, intermolecular slip is a major mechanism of dissipation (see, for instance in Fig. 8.36).

To enable this dissipation mechanism, the adhesion energy between HA crystals and tropocollagen molecules must be in a critical regime. This regime is characterized by the following condition: It must allow strengthening by making it more difficult to initiate molecular slip, but it must be small enough so that covalent bonds inside the tropocollagen molecules are not broken. Interface energies on the order

of magnitude that allow for these deformation mechanisms correspond to ionic interactions across the TC–HA interface. Indeed, ionic interactions have recently been suggested based on NMR studies of a TC–HA interface in physiological bone (Jaeger et al. 2005; Wilson et al. 2006).

Pure vdW or H-bond interactions would lead to adhesion energies of approximately $0.01\,\mathrm{J/m^2}$. This would be insufficient to make MCFs stronger or increase its toughness, thus rendering the presence of minerals in the gap regions insignificant. In the other extreme case, increasing $\gamma_{\mathrm{MF–TC}}$ to values corresponding to covalent bonds ($\gamma_{\mathrm{MF–TC}} > 1\,\mathrm{J/m^2}$), the deformation mechanics changes so that plastic yield does not set in until tropocollagen molecule rupture occurs, leading to a shutdown of the toughening mechanism.

The large aspect ratio of the mineral platelets leads to large shear forces between the tropocollagen molecule and the HA crystal, since $F_{\mathrm{shear}} \sim A_{\mathrm{C}}$ (the variable $A_{\mathrm{C}} \sim L_{\mathrm{C}}$ is the contact area between tropocollagen and HA).

The analysis of the strain distribution inside the MCF shows that the stress in HA platelets approaches several GPa. However, macroscopic HA crystals break at 0.1% tensile strain and stresses as low as 65 MPa. It was shown in earlier molecular simulation studies that by reducing the size of a HA crystal to dimensions below 30 nm, the strength of the crystal approaches the theoretical value, even under presence of cracks or other defects (Buehler et al. 2006). Under flaw-tolerant conditions, the material does not sense the existence of defects and is thus capable of reaching its theoretical strength. Thus the flaw-tolerance concept could be a possible explanation for the fact that mineral platelets can sustain large stresses that approach 1 GPa, without fracturing.

#### 8.5.4.2 Molecular Design Scenarios

Our model enables one to develop different design scenarios. As reported in a previous study, high cross-link densities in a pure CF without HA phase make the material stronger, but lead to a brittle polymer with low toughness and low stiffness. Such behavior is undesirable for the physiological role of bone.

As shown in the analyses reported in this chapter, adding very stiff ceramic platelets inside the collagen fibril represents a strategy to insert high densities of covalent chemistry in order to make the material stiffer and stronger without compromising toughness. The addition of mineral platelets allows the material to yield under large load in order to protect the entire structure. The molecular role of HA platelets in MCFs thus appears to be related to the increase of the strength by providing a larger energy barrier against intermolecular slip. At the same time, presence of HA platelets increases the dissipative nature of large-strain deformation of MCFs. Also, the molecular arrangement of MCFs allows to achieve a good weight–strength efficiency, since the dominating protein phase is lighter than the HA phase.

As discussed in a previous study (Buehler et al. 2006b), the length of tropocollagen molecules controls the mechanical behavior of CFs, and we expect a similar behavior for MCFs. Short tropocollagen molecules lead to reduced strength and MCFs may become rather brittle. Long tropocollagen molecules are vital to yield

large toughness, as they provide a means to enable long deformation paths with large slipping inside the material. The physiological significance of toughness may explain why extremely long tropocollagen molecules in MCFs is a highly conserved molecular feature. However, if tropocollagen molecules become too long, utilization of the intermolecular "glue" becomes inefficient. As shown in an earlier study (see also the discussion above), molecular lengths at approximately 200 nm provide an optimal basis for CFs. Further analysis of the dependence of mechanical properties of MCFs on the tropocollagen molecule length is left to future studies.

The molecular toughening mechanism described in this work unifies controversial attempts of explaining sources of toughness of bone, as it illustrates that both crack tip mechanisms and flaw tolerance concepts play a key role in the mechanical response of bone under extreme load.

In addition to mineralizing CFs, structural features at larger length scales of bone, the dependence of material properties on time (e.g., via osteoblast and osteoclast cells) and extrafibrillar matrix properties are important for the macroscopic mechanical properties of bone (Taylor et al. 2007). However, our results clearly show the significance of the nanoscale TC–HA patterning as a toughening mechanism at the nanoscale and microscale.

#### 8.5.4.3 Bone Formation and Tissue Growth

Our analysis shows that the particular properties of MCF allow to tolerate cracks at dimensions of several hundred micrometers; this may be critical to enable operation of basic molecular units (BMUs) in repair of bone, which require the presence of small cavities inside the tissue (Taylor et al. 2007).

The mechanical properties of a scaffolding material can influence the growth rate and quality of the bone tissue (Alsberg et al. 2006), providing evidence that not only chemical growth factors, but also the nanomechanical and micromechanical material properties play a role in tissue development.

Further, it has been shown that the presence of a stiff matrix directs stem cell differentiation toward osteoblasts (Engler et al. 2006). Thus the increase in stiffness due to mineralization – as shown in Fig. 8.35 and Table 8.4 – could be a critical aspect during formation of nascent bone.

### *8.5.5 Conclusion*

The studies reveal that the mechanical properties of CF change significantly after mineralization. Whereas pure tropocollagen fibrils are soft and the HA minerals are stiff and extremely fragile, the stiffness of mineralized fibrils assumes intermediate values, but with much increased energy dissipation during deformation (Table 8.4 summarizes the main effects of mineralization). Important structural features in MCFs and their effects on the mechanical behavior are :

- Presence of HA crystals, to provide additional resistance against plastic deformation, to increase Young's modulus and the fracture strength
- Adhesion forces between HA and tropocollagen remain weak enough, to allow for slip under large load instead of inducing fracture inside the tropocollagen molecules, but strong enough to provide significant strengthening
- Characteristic nanoscopic dimensions, to utilize the intermolecular adhesion forces most efficiently
- Further, as illustrated in a previous study (Buehler 2006b), presence of long tropocollagen molecules in order to provide the basis for long deformation paths for high energy dissipation

Modifications of the mechanical properties of CF under mineralization control the fracture properties of MCFs. Our analysis reveals that the particular constitutive behavior of MCFs induces a crack tip mechanism known as plastic shielding, effectively increasing the toughness of the tissue. The concept behind this mechanism is to sacrifice a small part of the structure in order to rescue the integrity of the entire structure. Presence of large yield regions on the order of several hundred micrometers leads to a more equal stress distribution under loading and enables operation of BMUs. In contrast, cracks in pure HA crystals lead to potentially dangerous large stress concentrations around flaws. The concept of equal stress distribution is known as a driving force for topology and shape evolution of natural structures such as bone and trees. The results suggest that this appears to be a universal principle that also holds at nanoscale.

Development of the yield region represents a toughening mechanism whose origin is intimately linked with molecular geometry and mechanisms, underlining the significance of nanostructure for bone properties. The results provide molecular scale explanations of experiments that show an increase in yield stress, maximum fracture stress, as well as failure strength with increasing mineral content.

## 8.6 Structure–Property Relationships in Biological Protein Materials

Historically, the classes of materials has been used to classify stages of civilizations, ranging from stone age more than 300,000 years ago to the bronze age, and possibly the silicon age in the late twentieth and early twenty-first century. However, a systematic analysis of materials in the context of linking chemical and physical concepts with engineering applications has not been achieved until very recently. For instance, 50 years ago, E. Orowan, M. Polanyi and G.I. Taylor have discovered dislocations, a concept proposed theoretically in 1905 by V. Volterra. It was discovered that dislocations represent the fundamental mechanism of plastic deformation of metals (Taylor 1934; Hirth and Lothe 1982). Remarkably, it was not until dislocations and other nanoscopic and microscopic mechanisms were understood theoretically that major breakthroughs have been possible that utilize this knowledge, to enable building high performance and reliable

airplanes, cars, space shuttles and more recently, nanodevices, through synthesis of ultra-strong and heat-resistant materials, for instance.

Perhaps, today we stand at another cross-road: Biological materials and systems are vital elements of life, and therefore, a rigorous understanding of the matter that makes life "work" is in reach. This may enable us eventually to integrate concepts from living systems into materials design, seamlessly. Optical, mechanical and electrical properties at ultra-small material scales, their control, synthesis and analysis as well as their theoretical description represent major scientific and engineering challenges and opportunities. However, just like in the case of more conventional materials, these breakthroughs will probably only be accessible provided that the fundamentals are understood very well. Characterization of the materials found in biology within a rigorous materials science approach is aimed toward the elucidation of these fundamental principles of assembly, deformation and fracture of these materials.

It is known from other fields in materials science that nanoscopic or microscopic structures control the macroscopic material behavior: For example, grain size reduction or confinement leads to an increase of the strength of crystalline metals (Nieh and Wadsworth 1991; Yip 1998; Blanckenhagen et al. 2001; Wolf et al. 2003). Deformation maps have been proposed to characterize material properties for engineering applications (Frost and Ashby 1982). Discovering similar insight for biological structures and materials represents an important frontier of research. A particularly challenging question is the elucidation of the significance and role of nanostructures for macroscopic properties, that is, carry out sensitivity analyses that show how small-scale features influence larger scale properties.

What are the most promising strategies in order to analyze these materials? Perhaps, an integrated approach that uses experiment and simulation concurrently could evolve into a new paradigm of materials research. Experimental techniques have gained unparalleled accuracy in both length and time scales (see Fig. 8.4), as reflected in development and utilization of atomic force microscope (AFM), optical tweezers or nanoindentation (Dao et al. 2003; Sun et al. 2004; Lim et al. 2006) to analyze biological materials. At the same time, modeling and simulation have evolved into predictive tools that complement experimental analyses (see Fig. 8.4) (Goddard 2006). It is now achievable to start from smallest scales – considering electrons and atoms – to reach all the way up to macroscopic scales of entire tissues (Goddard 2006), by explicitly considering the characteristic structural features at each scale. Even though there are still major challenges ahead of us, this progress is amazing and provides one with infinite possibilities and potentials, transforming materials science as a discipline through increased integration of computational approaches in scientific research (see Fig. 8.37).

### *8.6.1 Cross-Scale Interactions: Fracture Mechanisms in Collagenous Tissue*

Deformation and fracture are intimately linked to the atomic microstructure of the material. A central theme of the efforts in developing the materials science of

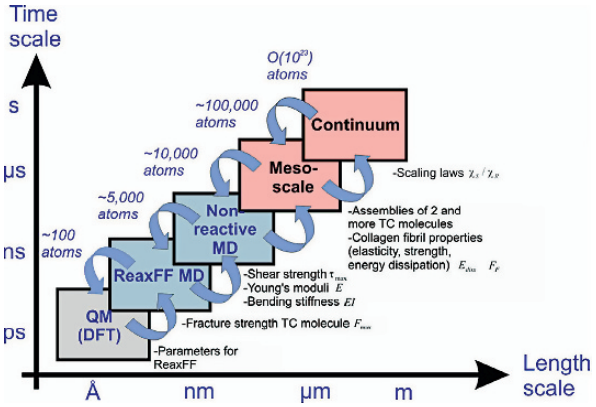


**Fig. 8.37** Summary of the multi-scale scheme used in this work. First principles quantum mechanics (QM) calculations (e.g., density function theory or DFT) are carried out to train a reactive force field ReaxFF. The reactive force field is used together with nonreactive force fields to obtain properties of individual TC molecules and assemblies of two TC molecules. Parameters include max $F$ (from ReaxFF), $E$, EI and shear $\tau$ (from nonreactive CHARMM). These parameters are used to develop a mesoscale model, which enables studies of ultra-long tropocollagen molecules and assemblies of those into collagen fibrils. The calculation results are coupled to the continuum scale using scaling laws. The scaling laws and associated length scales contain parameters that were obtained from mesoscale simulations (e.g., the length scale $\chi_S$)

biological materials is to appreciate the structure–property or structure-processing-property paradigm, constituting the heart of the materials science community. This paradigm has guided materials science for many decades. For biological materials, there are many challenges that make developing these rigorous links increasingly difficult.

For example, bond energies in biological materials are often comparable to the thermal energy, as for instance in the case of hydrogen bonding, the most abundant chemical bond in biology. Biological materials show highly viscoelastic behavior, since their response to mechanical deformation is intrinsically time dependent. In many cases, biological structures contain extremely compliant filaments, in which entropic contributions to free energy are important and can even control the deformation behavior. Many material properties are also length scale dependent and can vary significantly across various length scales. Quite often, this can be quite perplexing, since measuring different volumes of material leads to different values of Young's modulus. Size effects are very strong and possibly utilized systematically to ensure physiological functioning of the material in its biological context. However, why and how these size effects are exploited within this context remains less understood. The presence of hierarchical structures calls for new paradigms in thinking about the structure–property paradigm, since corresponding concepts must include an explicit notion of the cross-scale and inter-scale interactions.

It has become evident that the atomistic scale, and in particular the notion of a chemical bond, provides a very fundamental, universal platform at which a

variety of scientific disciplines can interact: chemists, through the molecular structure of proteins; physicists, through the statistical mechanics of a large number of atoms; and materials scientists through analysis of phenomena such as elasticity, optical properties, electrical properties or thermodynamics, linking structure and function.

A particularly exciting aspect of the materials science of biological materials is that it is interdisciplinary, by nature. Nature does not know of scientific disciplines, since they were invented by humans many centuries ago. Performing research in this field thus often means to overcome barriers between scientific disciplines and to develop strategies that enable us speak to each other more openly. Structures in universities and research institutions may have to be modified to facilitate such investigations.

It is vital to overcome the barrier that currently separates the scales, through development of new methods, better model systems and an advanced appreciation for a multi-scale view, in order to fully understand multi-scale or cross-scale interactions. To facilitate these developments, we must also develop a proper nomenclature to capture the various scales involved in a material. Current terminologies referring to atomistic, meso, micro and macro are insufficient to capture the subtleties of the various scales. Research should address the following questions: What are the opportunities in integrating nanoscience and nanotechnology into biological research? What will and can our impact be, in a long perspective, in understanding fundamental biology? For instance, is the nanomechanics of protein materials significant for biology, and have biologists missed out on important effects due to lack of consideration of the nanomechanics? How does Nature design materials that are environmentally friendly, lightweight and yet tough and robust and can serve multiple objectives? How is robustness achieved? How do universality and diversity integrate into biological structures?

From a theoretical viewpoint, major challenges are the development of new materials theories that include atomistic and statistical effects into an effective description, while retaining a system theoretical perspective, maybe eventually leading to a merger between system biology and materials science.

Similar to dislocation mechanics for metal plasticity, what is the theoretical framework for biological materials and structures? It is possible that statistical theories may evolve into the theoretical language of nanomechanics. Atomistic simulations of complex protein structures with explicit solvents are often prohibitive, and coarse-graining techniques are often used. However, how effective are coarse-graining techniques? Can we indeed average out over atomistic or mesoscale structures? How important are atomistic features at macroscale? What are the best numerical strategies to simulate the role of water in very small confinement? How does confined water influence the mechanics of natural and biological materials?

Progress in these various challenging fields will probably occur specific to problems and applications, perhaps in those which have most impact in medical or economic fields. Eventually, we must generalize our insight into the formulation of a *holistic theory* that extends the current nomenclature, theory and experimental thinking. These efforts will provide the scientific and engineering fundamentals to

develop and maintain the infrastructures to enable and evolve modern civilization. Materials – and materials science – will surely play a seminal role in these developments.

### *8.6.2 The Significance of Hierarchical Features*

A major trait of BPMs is the occurrence of hierarchies and the abundance of weak interactions. The presence of hierarchies in biological materials may be vital to take advantage of molecular and sub-molecular features, often characterized by weak interactions, and multiply their properties so that they become visible at larger scales. Utilization of weak interactions makes it possible to produce strong materials at moderate temperatures and thus with limited energy use.

Another distinction between traditional and biological materials is the geometrical occurrence of defects. While defects are often distributed randomly over the volume in crystalline materials, biological materials consist of an ordered structure that reaches down to the nanoscale. Defects are placed with atomistic or molecular precision and may play a major role in the material behavior observed at larger scales. These results suggest that analogies can be drawn between biological and synthetic materials.

In addition to the long-term impact in biology, bioengineering and medicine, this research may eventually contribute to our understanding of how different scales interact with one another. It may also enable synthesis of novel complex structural materials, designed from nano to macro. In order to achieve these goals, major challenges must be overcome, in particular in relating molecular processes to larger scale phenomena. As illustrated in this chapter for the example of collagenous tissues, protein materials constitute exceedingly complex structures. While the behavior of individual proteins is reasonably well understood, the properties of large assemblies of proteins remain largely unknown.

### *8.6.3 Universality Versus Diversity*

An important trait of protein materials is that they display highly specific hierarchical structures, from nano to macro. Some of these features are commonly found in different species and tissues, that is, they are highly conserved. Examples include alpha-helices, beta-sheets or collagen fibrils that represent universal building blocks forming the basis for diverse range of protein materials. In contrast, other features are highly specific to species or tissue types, such as tendon fascicles or beta-sheet nanocrystals in spider silk (Ackbarow and Buehler 2007a).

Universal features in protein materials are most common at nanoscale, as can be seen in examples such as the beta-strand motif, alpha-helices or collagen fibrils. Structural diversity becomes more prominent at larger scales. Biological materials often feature a coexistence of universality and diversity. Universality is linked to robustness, diversity is linked to optimality. The collagen fibril motif – one of the

most abundant protein structures found in biology – may be highly conserved since it provides a very robust means to achieve highly dissipative materials.

For instance, collagen consists of triple-helical tropocollagen molecules that have lengths of 300 nm with 1.5 nm in diameter. Staggered arrays of tropocollagen molecules form fibrils, which arrange to form collagen fibers. Whereas the fibrillar, staggered structure is a universal feature of collagenous tissue, structures at length scales beyond those of fibrils vary drastically for different species or different tissue. For instance, fibrils form fascicles in tendon, but mineralize to a hybrid composite in bone. In the eye's cornea, they align in a regular highly ordered orthogonal pattern. Universality persists up to the fibrillar level but vanishes at larger scales, when structural diversity dominates. Figure 8.38 depicts a schematic of the variation of structural features across the scales.

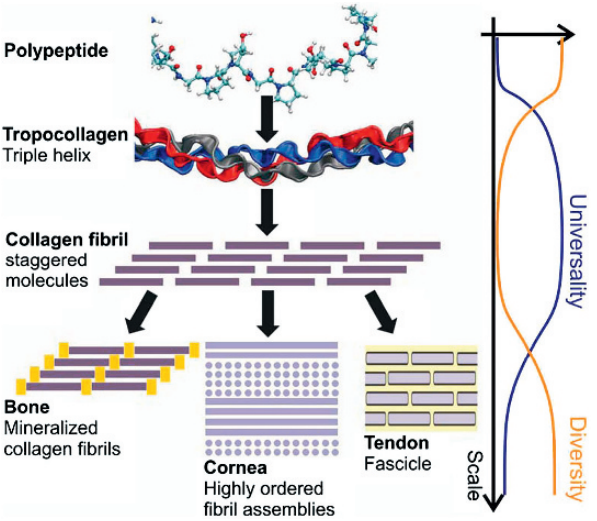


**Fig. 8.38** The nanostructure and microstructure of various collagen tissues, in light of the universality–diversity paradigm as discussed in Ackbarow and Buehler (2007a). Beyond the fibril scale, structural features vary significantly, here shown for bone, cornea and tendon

Notably, instead of creating a multitude of distinct secondary protein structures, Nature creates complexity through hierarchies and internal degrees of freedom that arise from the lower scale. Through applying hierarchies, Nature keeps the opportunity to adapt systems without significantly changing their structure. Formation of hierarchical structures enables one to overcome the physical limitations of a scale-specific design space. By simultaneously adapting a multitude of structures at different length scales, it is possible to create materials whose properties by far exceed those of each constituent or those that could be reached at a single scale alone. Understanding the fundamentals of this trait of biological materials could lay the foundation for a new class of biomimetic materials in which precisely controlled hierarchical features are exploited to tailor their properties.

## 8.7 Discussion and Conclusion

Deformation and fracture are fundamental phenomena with major implications on the stability and reliability of machines, buildings and biological systems. All deformation processes begin with erratic motion of individual atoms around flaws or defects that quickly evolve into formation of macroscopic fractures as chemical bonds rupture rapidly, eventually compromising the integrity of the entire structure. However, most existing theories of fracture treat matter as a continuum, neglecting the existence of atoms or nanoscopic features. Clearly, such a description is questionable. An atomistic approach as discussed in this chapter provides unparalleled insight into the complex atomic-scale deformation processes, linking nano to macro, without relying on empirical input.

The study reported here illustrates that molecular multi-scale modeling of collagen can be used to predict the elastic and fracture properties of hierarchical protein materials, marvelous examples of structural designs that balance a multitude of tasks, representing some of the most sustainable material solutions that integrate structure and function across the scales.

Breaking the material into its building blocks enables one to perform systematic studies of how microscopic design features influence the mechanical behavior at larger scales. The studies elucidate intriguing material concepts that balance strength, energy dissipation and robustness by selecting nanopatterned, hierarchical features.

Over the last century, engineers have developed understanding of how to create complex man-made structures out of a diverse range of constituents, at various scales (machines, buildings, airplanes, nuclear reactors and many others). Increased development and research funding into these areas of research will lead to breakthroughs not only on the fundamental sciences, but also in technological applications. Research in the area of mechanics of biological materials will extend our ability to carry out structural engineering, as used for buildings or bridges today, to the ultimate scale – nanoscale, and may be a vital component of the realization of nanotechnology.

A better understanding of the mechanics of biological and natural materials, integrated within complex technological systems, will make it possible to combine living and non-living environments to develop sustainable technologies. New materials technologies such as protein-based materials produced by recombinant DNA techniques represent new frontiers in materials design and synthesis (Langer and Tirrell 2004; Zhao and Zhang 2007). These questions have high impact on the understanding and design of environmentally friendly technologies and may enhance the quality of life of millions of people, through advances in the medical sciences as well as through improvements of the living environment. A currently pressing question is the development of new technologies to address the energy problem. Advances may be possible by utilization of bacteria to produce and process fuel from crops or by enabling the synthesis of materials at reduced processing temperature.

Nanoscience and nanotechnology enable us to make structures at the ultimate scale (self-assembly, recombinant DNA, utilization of motor proteins for

nanomachines and many others). This will perhaps lead to novel complex structural materials, designed from nano to macro. The theoretical progress in understanding hierarchical biological materials will facilitate to use an extended physical space, through the use of multiple hierarchies, in an efficient and controlled manner, that is, lead to a bottom-up structural design on the sub-macroscopic scale, instead of trial-and-error approaches. For example, the extended design space might serve as a means to realize new physical realities that are not accessible to a single scale, such as material synthesis at moderate temperatures, or fault-tolerant hierarchical assembly pathways (Cui et al. 2007; Hule and Pochan 2007; Winey 2007), which enable biological systems to overcome the limitations to particular chemical bonds (soft) and chemical elements (organic) present under natural conditions. The increased understanding of the hierarchical design laws might further enable the development and application of new organic and organic–inorganic multi-featured composites (such as assemblies of carbon nanotubes and proteins or polymer–protein composites (Petka et al. 1998; Langer and Tirrell 2004; Smeenk et al. 2005)), which will mainly consist of chemical elements that appear in our environment in an almost unlimited amount (C, H, N, O, S). These materials might consequently help to solve humans' energy and resource problems (e.g., fossil resources, iron, etc.) and allow us to manufacture nanomaterials, which will be produced in the future by techniques like recombinant DNA (Mershin et al. 2005; Zhao and Zhang 2006, 2007) or peptide self-assembly, techniques where the borders between materials, structures and machines vanish.

Applications of these new materials and structures are new biomaterials, new polymers, new composites, engineered spider silk, new scaffolding tissues, improved understanding of cell–ECM interactions, cell mechanics, hierarchical structures and self-assembly. In addition to the long-term impact in biology, bioengineering and medicine, this research may eventually contribute to our theoretical understanding of how structural features at different scales interact with one another. In light of the "extended physical design space" discussed above, this may transform engineering approaches not only for materials applications, but also in manufacturing, transportation or designs of networks.

**Acknowledgments** This research was supported by the Army Research Office (ARO), grant number W911NF-06-1-0291 (program officer Dr. Bruce LaMattina), the Solomon Buchsbaum AT&T Research Fund, as well as a National Science Foundation CAREER Award (CMMI-0642545, program officer Dr. Jimmy Hsia).

## References

Ackbarow, T. and M. J. Buehler (2007a). "Hierarchical coexistence of universality and diversity controls robustness and multi-functionality in protein materials" *Nature Precedings* http://hdl.nature.com/10101/npre.2007.826.1.

Ackbarow, T. and M. J. Buehler (2007). "Superelasticity, energy dissipation and strain hardening of vimentin coiled-coil intermediate filaments: Atomistic and continuum studies." *Journal of Materials Science* 42(21): 8771–8787. DOI 10.1007/s10853-007-1719-2.

Ackbarow, T., X. Chen, et al. (2007). "Hierarchies, multiple energy barriers and robustness govern the fracture mechanics of alpha-helical and beta-sheet protein domains." *Proceedings of the National Academy of Sciences of the USA* 104: 16410–16415.

Aizenberg, J., J. C. Weaver, et al. (2005). "Skeleton of Euplectella sp.: Structural hierarchy from the nanoscale to the macroscale." *Science* 309(5732): 275–278.

Alberts, B., A. Johnson, et al. (2002). *Molecular Biology of the Cell*, Taylor & Francis, London.

Allen, M. P. and D. J. Tildesley (1989). *Computer Simulation of Liquids*, Oxford University Press, Oxford.

Alsberg, E., H. J. Kong, et al. (2003). "Regulating bone formation via controlled scaffold degradation." *Journal of Dental Research* 82(11): 903–908.

An, K. N., Y. L. Sun, et al. (2004). "Flexibility of type I collagen and mechanical property of connective tissue." *Biorheology* 41(3–4): 239–246.

Anderson, T. L. (1991). *Fracture Mechanics: Fundamentals and Applications*, CRC Press, Boca Raton.

Anderson, D. (2005). Collagen Self-Assembly: A Complementary Experimental and Theoretical Perspective. Toronto, Canada, University of Toronto. PhD.

Arnoux, P. J., J. Bonnoit, et al. (2002). "Numerical damage models using a structural approach: Application in bones and ligaments." *European Physical Journal-Applied Physics* 17(1): 65–73.

Bailey, A. J. (2001). "Molecular mechanisms of ageing in connective tissues." *Mechanisms of Ageing and Development* 122(7): 735–755.

Bailey, N. P. and J. P. Sethna (2003). "Macroscopic measure of the cohesive length scale: Fracture of notched single-crystal silicon." *Physical Review B* 68(20).

Bell, G. I. (1978). "Models for specific adhesion of cells to cells." *Science* 200(4342): 618–627.

Bhattacharjee, A. and M. Bansal (2005). "Collagen structure: The Madras triple helix and the current scenario." *IUBMB Life* 57(3): 161–172.

Bischoff, J. E., E. M. Arruda, et al. (2000). "Finite element modeling of human skin using an isotropic, nonlinear elastic constitutive model." *Journal of Biomechanics* 33(6): 645–652.

Blanckenhagen, B. v., P. Gumbsch, et al. (2001). "Dislocation sources in discrete dislocation simulations of thin film plasticity and the Hall-Petch relation." *Modelling and Simulation in Materials Science and Engineering* 9: 157–169.

Borel, J. P. and J. C. Monboisse (1993). "Collagens – Why such a complicated structure." *Comptes Rendus Des Seances De La Societe De Biologie Et De Ses Filiales* 187(2): 124–142.

Borsato, K. S. and N. Sasaki (1997). "Measurement of partition of stress between mineral and collagen phases in bone using X-ray diffraction techniques." *Journal of Biomechanics* 30(9): 955–957.

Bozec, L. and M. Horton (2005). "Topography and mechanical properties of single molecules of type I collagen using atomic force microscopy." *Biophysical Journal* 88(6): 4223–4231.

Bozec, L. et al. (2005). "Atomic force microscopy of collagen structure in bone and dentine revealed by osteoclastic resorption. *Ultramicroscopy* 105: 79–89.

Brenner, D. W., O. A. Shenderova, et al. (2002). "A second-generation reactive empirical bond order (REBO) potential energy expression for hydrocarbons." *Journal Of Physics-Condensed Matter* 14(4): 783–802.

Broberg, K. B. (1990). *Cracks and Fracture*, Academic Press, New York.

Buehler, M. J. (2006a). "Atomistic and continuum modeling of mechanical properties of collagen: Elasticity, fracture and self-assembly." *Journal of Materials Research* 21(8): 1947–1961.

Buehler, M. J. (2006b). "Nature designs tough collagen: Explaining the nanostructure of collagen fibrils." *Proceedings of the National Academy of Sciences of the USA* 103(33): 12285–12290.

Buehler, M. J. (2007a). "Hierarchical chemo-nanomechanics of stretching protein molecules: Entropic elasticity, protein unfolding and molecular fracture." *Journal of Mechanics of Materials and Structures* 2(6): 1019–1057.

Buehler, M. J. (2007b). "Molecular nanomechanics of nascent bone: fibrillar toughening by mineralization." *Nanotechnology* 18: 295102.

Buehler, M. J. (2007). "Nano- and micromechanical properties of hierarchical biological materials and tissues" *Journal of Materials Science* 42(21): 8765–8770. DOI 10.1007/s10853-007-1952-8.

Buehler, M. J. (2008). "Nanomechanics of collagen fibrils under varying cross-link densities: Atomistic and continuum studies." *Journal of the Mechanical Behavior of Biomedical Materials* 1(1): doi:10.1016/j.jmbbm.2007.04.001

Buehler, M. J., F. F. Abraham, et al. (2003). "Hyperelasticity governs dynamic fracture at a critical length scale." *Nature* 426: 141–146.

Buehler, M. J., F. F. Abraham, et al. (2004). "Stress and energy flow field near a rapidly propagating mode I crack." *Springer Lecture Notes in Computational Science and Engineering* ISBN 3-540-21180-2: 143–156.

Buehler, M. J. and T. Ackbarow (2007). "Fracture mechanics of protein materials." *Materials Today* 10(9): 46–58.

Buehler, M. J., J. Dodson, et al. (2006). "The Computational Materials Design Facility (CMDF): A powerful framework for multiparadigm multi-scale simulations." *Materials Research Society Symposium Proceedings* 894: LL3.8.

Buehler, M. J., A. C. T. v. Duin, et al. (2006). "Multi-paradigm modeling of dynamical crack propagation in silicon using the ReaxFF reactive force field." *Physical Review Letters* 96(9): 095505.

Buehler, M. J. and H. Gao (2006). "Dynamical fracture instabilities due to local hyperelasticity at crack tips" *Nature* 439: 307–310.

Buehler, M. J., H. Tang, et al. (2007). "Threshold crack speed controls dynamical fracture of silicon single crystals." *Physical Review Letters*. 99: 165502.

Buehler, M. J. and S. Y. Wong (2007). "Entropic elasticity controls nanomechanics of single tropocollagen molecules." *Biophysical Journal* 93(1): 37–43.

Buehler, M. J., H. Yao, et al. (2006). "Cracking and adhesion at small scales: atomistic and continuum studies of flaw tolerant nanostructures." *Modelling and Simulation in Materials Science and Engineering* 14: 799–816.

Bustamante, C., J. F. Marko, et al. (1994). "Entropic elasticity of lambda-phage DNA." *Science* 265(5178): 1599–1600.

Chenoweth, K., S. Cheung, et al. (2005). "Simulations on the thermal decomposition of a poly(dimethylsiloxane) polymer using the ReaxFF reactive force field." *Journal of the American Chemical Society* 127(19): 7192–7202.

Cheung, S., W. Q. Deng, et al. (2005). "ReaxFF(MgH) reactive force field for magnesium hydride systems." *Journal of Physical Chemistry A* 109(5): 851–859.

Courtney, T. H. (1990). *Mechanical Behavior of Materials*. New York, NY, USA, McGraw-Hill.

Cressey, B. A. and G. Cressey (2003). "A model for the composite nanostructure of bone suggested by high-resolution transmission electron microscopy." *Mineralogical Magazine* 67(6): 1171–1182.

Cui, X. Q., C. M. Li, et al. (2007). "Biocatalytic generation of ppy-enzyme-CNT nanocomposite: From network assembly to film growth." *Journal of Physical Chemistry C* 111(5): 2025–2031.

Currey, J. D. (2002). *Bones: Structure and Mechanics*. Princeton, NJ, Princeton University Press.

Currey, J. D. (2005). "Materials science – Hierarchies in biomineral structures." *Science* 309(5732): 253–254.

Cusack, S. and A. Miller (1979). "Determination of the elastic-constants of collagen by Brillouin light-scattering." *Journal of Molecular Biology* 135(1): 39–51.

Cuy, J. L., A. B. Mann, et al. (2002). "Nanoindentation mapping of the mechanical properties of human molar tooth enamel." *Archives of Oral Biology* 47(4): 281–291.

Dao, M., C. T. Lim, et al. (2003). "Mechanics of the human red blood cell deformed by optical tweezers." *Journal of the Mechanics and Physics of Solids* 51(11–12): 2259–2280.

Dao, M., C. T. Lim, et al. (2005). "Mechanics of the human red blood cell deformed by optical tweezers (vol 51, pg 2259, 2003)." *Journal of the Mechanics and Physics of Solids* 53(2): 493–494.

Datta, D., A. C. T. v. Duin, et al. (2005). "Extending ReaxFF to biomacromolecules." *Unpublished*.
Duin, A. C. T. v., S. Dasgupta, et al. (2001). "ReaxFF: A reactive force field for hydrocarbons." *Journal of Physical Chemistry A* 105: 9396–9409.
Duin, A. C. T. v., A. Strachan, et al. (2003). "ReaxFF SiO: Reactive force field for silicon and silicon oxide systems." *Journal of Physical Chemistry A* 107: 3803–3811.
Engler, A. J., S. Sen, et al. (2006). "Matrix elasticity directs stem cell lineage specification." *Cell* 126(4): 677–689.
Eppell, S. J., B. N. Smith, et al. (2006). "Nano measurements with micro-devices: mechanical properties of hydrated collagen fibrils." *Journal of the Royal Society Interface* 3(6): 117–121.
Ercolessi, F. and J. B. Adams (1994). "Interatomic potentials from 1st principle-calculations – the force matching method." *Europhysics Letter* 28(8): 583–588.
Fantner, G. E., T. Hassenkam, et al. (2005). "Sacrificial bonds and hidden length dissipate energy as mineralized fibrils separate during bone fracture." *Nature Materials* 4(8): 612–616.
Fratzl, P., H. S. Gupta, et al. (2004). "Structure and mechanical quality of the collagen-mineral nano-composite in bone." *Journal of Materials Chemistry* 14(14): 2115–2123.
Fratzl, P. and R. Weinkamer (2007). "Nature's hierarchical materials." *Progress in Materials Science* 52: 1263–1334.
Freeman, J. W. and F. H. Silver (2004). "Elastic energy storage in unmineralized and mineralized extracellular matrices (ECMs): A comparison between molecular modeling and experimental measurements." *Journal of Theoretical Biology* 229(3): 371–381.
Freund, L. B. (1990). *Dynamic Fracture Mechanics*, Cambridge University Press, Cambridge, ISBN 0-521-30330-3.
Frost, H. J. and M. F. Ashby (1982). *Deformation-mechanism Maps*, Pergamon Press, Oxford.
Gao, H. J. (2006). "Application of fracture mechanics concepts to hierarchical biomechanics of bone and bone-like materials." *International Journal of Fracture* 138(1–4): 101–137.
Gao, H., B. Ji, et al. (2003). "Materials become insensitive to flaws at nanoscale: Lessons from nature." *Proceedings of the National Academy Sciences of the USA* 100(10): 5597–5600.
Glorieux, F. H. (2005). "Caffey disease: An unlikely collagenopathy." *Journal of Clinical Investigation* 115(5): 1142–1144.
Goddard, W. A. (2006). A Perspective of Materials Modeling *Handbook of Materials Modeling*. S. Yip, Springer.
Grandbois, M., M. Beyer, et al. (1999). "How strong is a covalent bond?" *Science* 283(5408): 1727–1730.
Griffith, A. A. (1920). "The phenomenon of rupture and flows in solids." *Philosophical Transactions of the Royal Society of London, Series A* 221: 163–198.
Gropp, W., W. Lusk, et al. (1999). *Using MPI*, MIT Press, Cambridge.
Gupta, H. S., P. Messmer, et al. (2004). "Synchrotron diffraction study of deformation mechanisms in mineralized tendon." *Physical Review Letters* 93(15).
Gupta, H. S., J. Seto, et al. (2006). "Cooperative deformation of mineral and collagen in bone at the nanoscale." *Proceedings of the National Academy Sciences of the USA* 103: 17741–17746.
Gupta, H. S., W. Wagermaier, et al. (2005). "Nanoscale deformation mechanisms in bone." *Nano Letters* 5(10): 2108–2111.
Han, S. S., A. C. T. van Duin, et al. (2005). "Optimization and application of lithium parameters for the reactive force field, ReaxFF." *Journal of Physical Chemistry A* 109(20): 4575–4582.
Hansma, P. K., P. J. Turner, et al. (2007). "Optimized adhesives for strong, lightweight, damage-resistant, nanocomposite materials: New insights from natural materials." *Nanotechnology* 18(4).
Harley, R., D. James, et al. (1977). "Phonons and elastic-moduli of collagen and muscle." *Nature* 267(5608): 285–287.
Hellan, K. (1984). *Introduction to Fracture Mechanics*, McGraw-Hill, Inc., New York.
Hellmich, C. and F. J. Ulm (2002). "Are mineralized tissues open crystal foams reinforced by crosslinked collagen? – some energy arguments." *Journal of Biomechanics* 35(9): 1199–1212.

Hirth, J. P. and J. Lothe (1982). *Theory of Dislocations*, Wiley-Interscience, New York.
Hofmann, H., T. Voss, et al. (1984). "Localization of flexible sites in thread-like molecules from electron-micrographs – comparison of interstitial, basement-membrane and intima collagens." *Journal of Molecular Biology* 172(3): 325–343.
Holland, J. H. (1995). *Hidden Order – How Adaptation Builds Complexity*. Reading, MA, Helix Books. http://www.top500.org/ TOP 500 Supercomputer Sites.
Hule, R., A., Pochan, D., J., (2007). "Polymer nanocomposites for biomedical application." *MRS Bulletin* 32(4): 5.
Hulmes, D. J. S., T. J. Wess, et al. (1995). "Radial packing, order, and disorder in collagen fibrils." *Biophysical Journal* 68(5): 1661–1670.
Humphrey, W., A. Dalke, et al. (1996). "VMD: Visual molecular dynamics." *Journal of Molecular Graphics* 14(1): 33.
Israelowitz, M., S. W. H. Rizvi, et al. (2005). "Computational modeling of type I collagen fibers to determine the extracellular matrix structure of connective tissues." *Protein Engineering Design & Selection* 18(7): 329–335.
Jaeger, C., N. S. Groom, et al. (2005). "Investigation of the nature of the protein-mineral interface in bone by solid-state NMR." *Chemistry of Materials* 17(12): 3059–3061.
Jager, I. and P. Fratzl (2000). "Mineralized collagen fibrils: A mechanical model with a staggered arrangement of mineral particles." *Biophysical Journal* 79(4): 1737–1746.
Kadau, K., T. C. Germann, et al. (2004). "Large-scale molecular-dynamics simulation of 19 billion particles." *International Journal of Modern Physics C* 15: 193.
Kim, B. S., J. Nikolovski, et al. (1999). "Cyclic mechanical strain regulates the development of engineered smooth muscle tissue." *Nature Biotechnology* 17(10): 979–983.
Kramer, R. Z., M. G. Venugopal, et al. (2000). "Staggered molecular packing in crystals of a collagen-like peptide with a single charged pair." *Journal of Molecular Biology* 301(5): 1191–1205.
Lakes, R. (1993). "Materials with structural hierarchy." *Nature* 361(6412): 511–515.
Laudis, W., B. L. H. Kraus, et al. (2002). "Vascular-mineral spatial correlation in the calcifying turkey leg tendon." *Connective Tissue Research* 43(4): 595–605.
Langer, R. and D. A. Tirrell (2004). "Designing materials for biology and medicine." *Nature* 428(6982): 487–492.
Lantz, M. A., H. J. Hug, et al. (2001). "Quantitative measurement of short-range chemical bonding forces." *Science* 291(5513): 2580–2583.
Layton, B. E., S. M. Sullivan, et al. (2005). "Nanomanipulation and aggregation limitations of self-assembling structural proteins." *Microelectronics Journal* 36(7): 644–649.
Lees, S. (1987). "Possible effect between the molecular packing of collagen and the composition of bony tissues." *International Journal Of Biological Macromolecules* 9(6): 321–326.
Lees, S. (2003). "Mineralization of type I collagen." *Biophysical Journal* 85(1): 204–207.
Lichtens Jr, G. R. Martin, et al. (1973). "Defect in conversion of procollagen to collagen in a form of Ehlers-Danlos syndrome." *Science* 182(4109): 298–300.
Lim, C. T., E. H. Zhou, et al. (2006). "Experimental techniques for single cell and single molecule biomechanics." *Materials Science & Engineering C-Biomimetic and Supramolecular Systems* 26(8): 1278–1288.
Lodish, H. B., Arnold; Zipursky, S. Lawrence; Matsudaira, Paul; Baltimore, David; Darnell, James E. (1999). *Molecular Cell Biology*. W H Freeman & Co, New York.
Lorenzo, A. C. and E. R. Caffarena (2005). "Elastic properties, Young's modulus determination and structural stability of the tropocollagen molecule: a computational study by steered molecular dynamics." *Journal of Biomechanics* 38(7): 1527–1533.
Lotz, J. C., T. N. Gerhart, et al. (1990). "Mechanical-properties of trabecular bone from the proximal femur – a quantitative Ct study." *Journal of Computer Assisted Tomography* 14(1): 107–114.
Louis, O., F. Boulpaep, et al. (1995). "Cortical mineral-content of the radius assessed by peripheral qct predicts compressive strength on biomechanical testing." *Bone* 16(3): 375–379.

Lu, H., B. Isralewitz, et al. (1998). "Unfolding of titin immunoglobulin domains by steered molecular dynamics simulation." *Biophysical Journal* 75(2): 662–671.
MacKerell, A. D., D. Bashford, et al. (1998). "All-atom empirical potential for molecular modeling and dynamics studies of proteins." *Journal of Physical Chemistry B* 102(18): 3586–3616.
Mershin, A., B. Cook, et al. (2005). "A classic assembly of nanobiomaterials." *Nature Biotechnology* 23(11): 1379–1380.
Miles, C. A. and A. J. Bailey (2001). "Thermally labile domains in the collagen molecule." *Micron* 32(3): 325–332.
Mooney, S. D., C. C. Huang, et al. (2001). "Computed free energy differences between point mutations in a collagen-like peptide." *Biopolymers* 58(3): 347–353.
Mooney, S. D. and T. E. Klein (2002). "Structural models of osteogenesis imperfecta-associated variants in the COL1A1 gene." *Molecular & Cellular Proteomics* 1(11): 868–875.
Mooney, S. D., P. A. Kollman, et al. (2002). "Conformational preferences of substituted prolines in the collagen triple helix." *Biopolymers* 64(2): 63–71.
Nalla, R. K., J. H. Kinney, et al. (2003a). "Effect of orientation on the in vitro fracture toughness of dentin: the role of toughening mechanisms." *Biomaterials* 24(22): 3955–3968.
Nalla, R. K., J. H. Kinney, et al. (2003b). "Mechanistic fracture criteria for the failure of human cortical bone." *Nature Materials* 2(3): 164–168.
Nalla, R. K., J. J. Kruzic, et al. (2005). "Mechanistic aspects of fracture and R-curve behavior in human cortical bone." *Biomaterials* 26(2): 217–231.
Nalla, R. K., J. S. Stolken, et al. (2005). "Fracture in human cortical bone: local fracture criteria and toughening mechanisms." *Journal of Biomechanics* 38(7): 1517–1525.
Nelson, M. T., W. Humphrey, et al. (1996). "NAMD: A parallel, object oriented molecular dynamics program." *International Journal Of Supercomputer Applications And High Performance Computing* 10(4): 251–268.
Nieh, T. G. and J. Wadsworth (1991). "Hall-Petch relation in nanocrystalline solids." *Scripta Metallurgica* 25(4).
Nielson, K. D., A. C. T. v. Duin, et al. (2005). "Development of the ReaxFF reactive force field for describing transition metal catalyzed reactions, with application to the initial stages of the catalytic formation of carbon nanotubes." *Journal of Physical Chemistry A* 109: 49.
Orgel, J. P. R. O., T. C. Irving, et al. (1995). "Microfibrillar structure of type I collagen in situ." *Proceedings of the National Academy Sciences of the USA* 103(24): 9001–9005.
Persikov, A. V., J. A. M. Ramshaw, et al. (2005). "Electrostatic interactions involving lysine make major contributions to collagen triple-helix stability." *Biochemistry* 44(5): 1414–1422.
Peterlik, H., P. Roschger, et al. (2006). "From brittle to ductile fracture of bone." *Nature Materials* 5(1): 52–55.
Petka, W. A., J. L. Harden, et al. (1998). "Reversible hydrogels from self-assembling artificial proteins." *Science* 281(5375): 389–392.
Phillips, J. C., R. Braun, et al. (2005). "Scalable molecular dynamics with NAMD." *Journal of Computational Chemistry* 26(16): 1781–1802.
Plimpton, S. (1995). "Fast parallel algorithms for short-range molecular-dynamics." *Journal of Computational Physics* 117: 1–19.
Prater, C. B., H. J. Butt, et al. (1990). "Atomic force microscopy." *Nature* 345(6278): 839–840.
Puxkandl, R., I. Zizak, et al. (2002). "Viscoelastic properties of collagen: Synchrotron radiation investigations and structural model." *Philosophical Transactions of the Royal Society of London Series B-Biological Sciences* 357(1418): 191–197.
Ramachandran, G. N., Kartha, G. (1955). "Structure of collagen." *Nature* 176: 593–595.
Rappé, A. K. and W. A. Goddard (1991). "Charge equilibration for molecular-dynamics simulations." *Journal of Physical Chemistry* 95(8): 3358–3363.
Rief, M., M. Gautel, et al. (1997). "Reversible unfolding of individual titin immunoglobulin domains by AFM." *Science* 276(5315): 1109–1112.

Ritchie, R. O., J. J. Kruzic, et al. (2004). "Characteristic dimensions and the micro-mechanisms of fracture and fatigue in 'nano' and 'bio' materials." *International Journal of Fracture* 128(1–4): 1–15.

Ritchie, R. O., R. K. Nalla, et al. (2006). "Fracture and ageing in bone: Toughness and structural characterization." *Strain* 42(4): 225–232.

Robins, S. P. and A. J. Bailey (1973). "The chemistry of the collagen cross-links." *Biochemical Journal*. 135: 657–665.

Sasaki, N. and S. Odajima (1996). "Elongation mechanism of collagen fibrils and force-strain relations of tendon at each level of structural hierarchy." *Journal of Biomechanics* 29(9): 1131–1136.

Screen, H. R. C., D. L. Bader, et al. (2004). "Local strain measurement within tendon." *Strain* 40(4): 157–163.

Smeenk, J. M., M. B. J. Otten, et al. (2005). "Controlled assembly of macromolecular beta-sheet fibrils." *Angewandte Chemie-International Edition* 44(13): 1968–1971.

Smith, B. L., T. E. Schaffer, et al. (1999). "Molecular mechanistic origin of the toughness of natural adhesives, fibres and composites." *Nature* 399(6738): 761–763.

Strachan, A., E. M. Kober, et al. (2005). "Thermal decomposition of RDX from reactive molecular dynamics." *Journal of Chemical Physics* 122(5): 054502.

Strachan, A., A. C. T. van Duin, et al. (2003). "Shock waves in high-energy materials: The initial chemical events in nitramine RDX." *Physical Review Letters* 91(9): 098301.

Stuart, S. J., A. B. Tutein, et al. (2000). "A reactive potential for hydrocarbons with intermolecular interactions." *Journal of Chemical Physics* 112(14): 6472-6486.

Sun, Y. L., Z. P. Luo, et al. (2002). "Direct quantification of the flexibility of type I collagen monomer." *Biochemical and Biophysical Research Communications* 295(2): 382–386.

Sun, Y. L., Z. P. Luo, et al. (2004). "Stretching type II collagen with optical tweezers." *Journal of Biomechanics* 37(11): 1665–1669.

Tai, K., F. J. Ulm, et al. (2006). "Nanogranular origins of the strength of bone." *Nano Letters* 11: 2520–2525

Taylor, G. I. (1934). "Mechanism of plastic deformation in crystals." *Proceedings of the Royal Society A* 145: 362.

Taylor, D., J.G. Hazenberg, et al. (2007). "Living with cracks: Damage and repair in human bone." *Nature Materials* 6(4): 263–266.

Thompson, J. B., J. H. Kindt, et al. (2001). "Bone indentation recovery time correlates with bond reforming time." *Nature* 414(6865): 773–776.

Tsai, D. H. (1979). "Virial theorem and stress calculation in molecular-dynamics." *Journal of Chemical Physics* 70(3): 1375–1382.

Turner, C. H. (2006). Bone strength: Current concepts. *Skeletal Development and Remodeling in Health, Disease, and Aging*. 1068: 429–446.

van der Rijt, J. A. J., K. O. van der Werf, et al. (2006). "Micromechanical testing of individual collagen fibrils." *Macromolecular Bioscience* 6(9): 697–702.

van Duin, A. C. T., K. Nielson, et al. (2004). "Application of ReaxFF reactive force fields to transition metal catalyzed nanotube formation." *Abstracts of Papers of the American Chemical Society* 227: U1031–U1031.

Vesentini, S., C. F. C. Fitie, et al. (2005). "Molecular assessment of the elastic properties of collagen-like homotrimer sequences." *Biomechanics and Modeling in Mechanobiology* 3(4): 224–234.

Wachter, N. J., G. D. Krischak, et al. (2002). "Correlation of bone mineral density with strength and microstructural parameters of cortical bone in vitro." *Bone* 31(1): 90–95.

Waite, J. H., X. X. Qin, et al. (1998). "The peculiar collagens of mussel byssus." *Matrix Biology* 17(2): 93–106.

Weiner, S. and H. D. Wagner (1998). "The material bone: Structure mechanical function relations." *Annual Review of Materials Science* 28: 271–298.

Wilson, E. E., A. Awonusi, et al. (2006). "Three structural roles for water in bone observed by solid-state NMR." *Biophysical Journal* 90(10): 3722–3731.
Winey, K. I., Vaia R.A., (2007). "Polymer nanocomposites." *MRS Bulletin* 32(4): 5.
Wolf, D., V. Yamakov, et al. (2003). "Deformation mechanism and inverse Hall-Petch behavior in nanocrystalline materials." *Zeitschrift Fur Metallkunde* 94: 1052–1061.
Yip, S. (1998). "The strongest size." *Nature* 391: 532–533.
Zervakis, M., V. Gkoumplias, et al. (2005). "Analysis of fibrous proteins from electron microscopy images." *Medical Engineering & Physics* 27(8): 655–667.
Zhao, X. J. and S. G. Zhang (2006). "Molecular designer self-assembling peptides." *Chemical Society Reviews* 35(11): 1105–1110.
Zhao, X. J. and S. G. Zhang (2007). "Designer self-assembling peptide materials." *Macromolecular Bioscience* 7(1): 13–22.
Zhu, W. H. and P. Wu (2004). "Surface energetics of hydroxyapatite: a DFT study." *Chemical Physics Letters* 396(1–3): 38–42.
Zimmerman, J. A., E. B. Webb, et al. (2004). "Calculation of stress in atomistic simulation." *Modelling and Simulation in Materials Science and Engineering* 12: S319–S332.